


5-2024

Use of Molecular Logic Gates for the Tuning of Chemosensor Dynamic Range

Orhan Acikgoz
William & Mary

Follow this and additional works at: <https://scholarworks.wm.edu/honorsthesis>

 Part of the [Analytical Chemistry Commons](#), [Organic Chemistry Commons](#), and the [Physical Chemistry Commons](#)

Recommended Citation

Acikgoz, Orhan, "Use of Molecular Logic Gates for the Tuning of Chemosensor Dynamic Range" (2024). *Undergraduate Honors Theses*. William & Mary. Paper 2127.
<https://scholarworks.wm.edu/honorsthesis/2127>

This Honors Thesis -- Open Access is brought to you for free and open access by the Theses, Dissertations, & Master Projects at W&M ScholarWorks. It has been accepted for inclusion in Undergraduate Honors Theses by an authorized administrator of W&M ScholarWorks. For more information, please contact scholarworks@wm.edu.

Use of Molecular Logic Gates for the Tuning of Chemosensor Dynamic Range

A thesis presented in Candidacy for Departmental Honors in

Chemistry

from

The College of William and Mary in Virginia

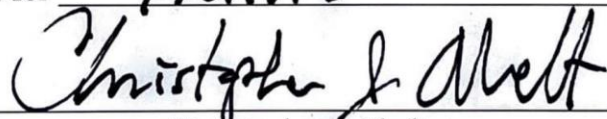
By

Orhan Acikgoz

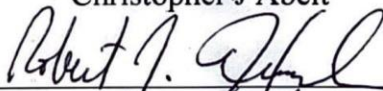
May 8, 2024

Accepted for

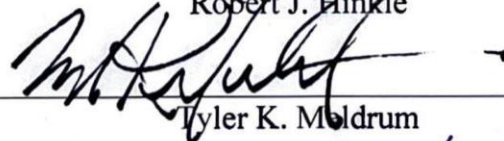
Honors



Christopher J. Abelt



Robert J. Hinkle



Tyler K. Moldrum



Helen Murphy

Table of Contents

Abstract	1
Introduction	2
Fluorescence.....	2
Chemosensors	4
Dynamic Range	6
Naphthalimide Chemosensors	7
Molecular Logic Gates	8
Purpose of Our Study	10
Methods	12
Organic Synthesis	12
Experimental	14
Failed Pathways	23
4,5-Substituted Naphthalimide.....	23
1-Aza-15-Crown-5.....	25
Extension of The Crown With A Spacer.....	26
Results	27
Absorption Spectroscopy	27
Fluorescence Spectroscopy	29
Binding Constant.....	31
Detection Limit	35
Conclusions	36
Interpretation of Results	36
Limitations.....	36
Future Research	37
References	39
Images	41
Appendix	42

Abstract

The first molecular logic gates were created in the 1990s; integrating such logic gates into fluorescent chemosensors allowed for the detection of different types of ions in solution. In this study, we have developed a new use of molecular logic gates by having two of the same type of binding site. The two binding sites on a fluorophore that both detect Na^+ ions led to an increase in the detection limit compared with the chemosensor with a single binding site. Since the two sodium binding sites create an AND logic gate, two sodium ions are needed to generate a fluorescence response whereas the single-input chemosensor only requires a single ion. Tuning the chemosensor dynamic range is an important problem that must be overcome for developing useful chemosensors, and our technique can be used to shift the dynamic range without the need for novel ligands and binding sites.

Introduction

Fluorescence

Molecules and atoms have discrete, electronic quantum levels. Excitation from ground level to a higher electronic level may occur upon the absorbance of light.^[1]

Fluorescence is a type of luminescence in which light is emitted as an excited system relaxes down to its ground state.^[2] There are several different ways for a system to relax down to the ground state, and most molecules are non-fluorescent and go through non-radiative relaxation, where the energy is lost as heat.

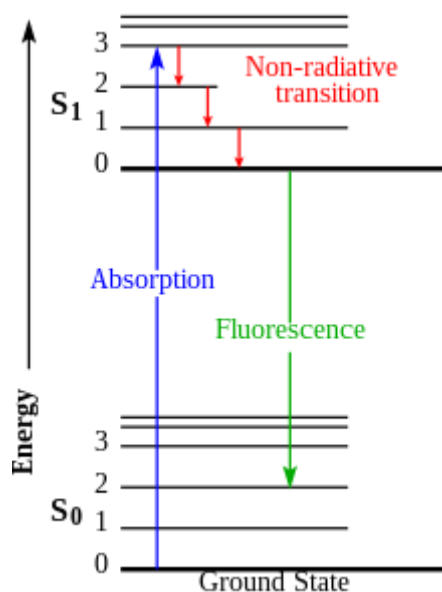


Figure 1: A Jablonski diagram depicting possible electronic transitions.^[16]

Since some fraction of the absorbed photon is released through non-radiative processes, the energy of the emitted photon will be lower energy and higher wavelength

compared to the photon that was absorbed. This difference in energy between absorbed and fluorescent light is called the Stokes shift. This has implications for fluorescence spectroscopy as it allows one to distinguish between the light source and the fluorescence response.^[4]

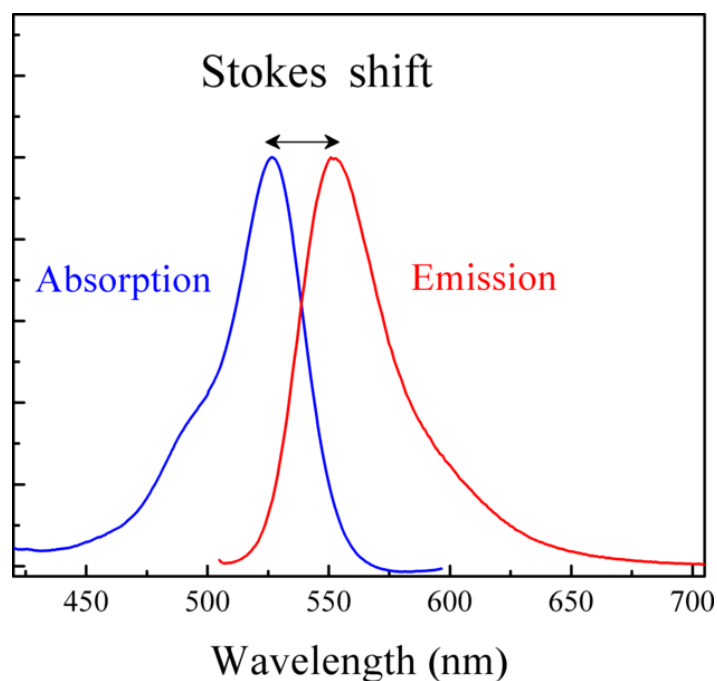


Figure 2: Stokes shift, the change in energy between absorbed and emitted light.^[17]

The ratio of photons emitted through fluorescence to photons absorbed is called the quantum yield. Different fluorescent molecules have different quantum yields based on the likelihood of fluorescence to other processes such as non-radiative relaxation, internal conversion, etc. Thus, quantum yield serves as a measure of fluorescence intensity and efficiency.

Chemosensors

Chemosensors are molecules that display a measurable change in their physical properties in response to changes in the environment. Fluorescent molecules can be engineered into chemosensors through various mechanisms. The general formula for the construction of such molecules includes a fluorophore (fluorescent molecule), an ionophore (binding site that detects a given analyte), and a spacer that allows the transmission of information between these two parts.^[3]

The binding site of a chemosensor can quench the fluorescence of a chemosensor through various processes. The most commonly employed mechanism is photoinduced electron transfer (PET), where an electronically excited molecule accepts an electron from the ionophore and relaxes down to its ground state. This leads to a quenching of the fluorescence as it is a non-radiative process. When an analyte binds to the receptor, however, PET is inhibited, which leads to an increase in fluorescence intensity. By measuring this change in fluorescence, it is possible to quantify a range of concentrations of a given analyte.^[13]

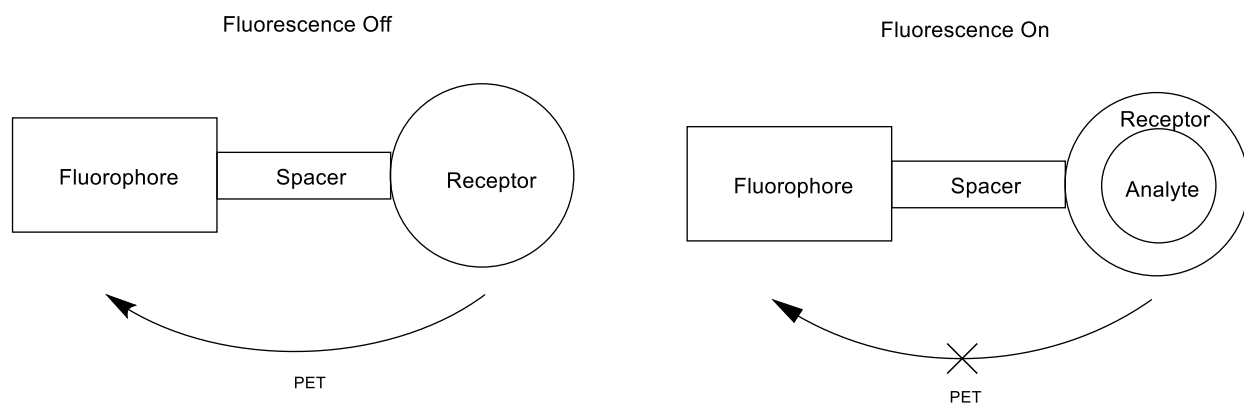


Figure 3: Photoinduced electron transfer forming the basis for many off-on chemosensors. The binding of the analyte inhibits the fluorescence quenching mechanism.

In the past decades, fluorescent chemosensors have gained a lot of interest due to their practicality in various fields such as cell biology, environmental sciences, and various other fields that require quantitative analysis. Through the customization of their binding site, chemosensors are designed to be chemoselective; for example, a sodium chemosensor will not be receptive to calcium ions due to the difference in the diameter between the analyte and the ionophore. Another advantage of chemosensors is that they allow for real-time imaging. Since most of the binding processes are reversible, one can quantify the decrease in analyte concentration just as they can with an increase. Details as such are crucial when studying a dynamic system like a biological cell. Due to these practical advantages, there is demand for the development of novel chemosensors while addressing problems such as chemoselectivity, dynamic range, solubility, etc.

Dynamic Range

A key problem in the development and use of chemosensors is the issue of dynamic range. The system that is being analyzed needs to have an analyte concentration that is within the dynamic range to do quantitative analysis. If the concentration is below the detection limit, the chemosensor will show no reasonable increase in fluorescence. Similarly, if the concentration is high enough to exceed the dynamic range, the chemosensor will always display maximum fluorescence. For this reason, different areas of research demand chemosensors with suitable dynamic ranges for that field.^[4] This demand may hold even within a field. A good example of this is a sodium chemosensor that was developed for sensing intracellular sodium concentration; this molecule could not be used to monitor extracellular sodium, which stands at a much higher concentration comparatively.^[5]

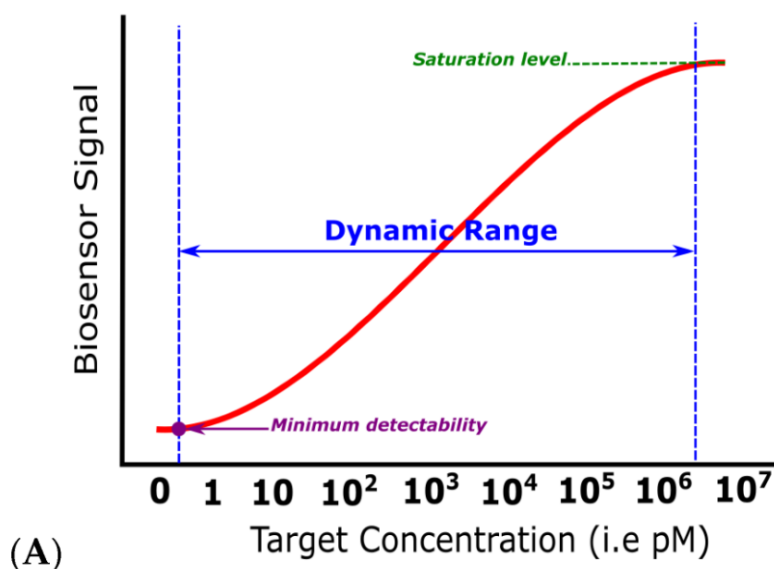


Figure 4: Depiction of the dynamic range of a chemosensor on a logarithmic scale. Detection limit and saturation points are also highlighted.^[18]

Naphthalimide Chemosensors

Various characteristics are sought after in the development and use of fluorescent chemosensors. These considerations render some fluorescent molecules and design strategies superior to others. 1,8-Naphthalimide derivatives make for good chemosensors due to various factors: (a) They make for great fluorophores due to their high quantum yield and large Stokes shift; (b) The absorption and emission wavelength of naphthalimide derivatives are in the visible region of the light spectrum; (c) Their solubility in both organic and aqueous solvents allow for them to be used in different fields.^[14] Many organic reactions have been reported in the literature, which allowed us to synthesize the two chemosensors through reliable pathways.

In addition, naphthalimide-based chemosensors have been used to create two-input AND logic gates in the path where the two binding sites were attached to the naphthalene and imide parts of the molecule. With these factors taken into consideration, we deemed naphthalimide derivatives to be the ideal candidate for this study.^[15]

Molecular Logic Gates

Logic gates are Boolean functions that are often employed in computer science. These functions allow one to perform operations where the output depends on one or more inputs.^[6] The most known examples of two input logic gates are the “AND” and “OR” logic gates. The former creates an output when both inputs are present, the latter will create the same output if one or the other input is present. The presence of an input or output is binary; since there are four different cases for each logic gate, there are a total of 16 (2^4) two input logic gates.








Input		Output (Q)						
								
A	B	AND	OR	INH	XOR	NAND	NOR	XNOR
0	0	0	0	0	0	1	1	1
0	1	0	1	0	1	1	0	0
1	0	0	1	1	1	1	0	0
1	1	1	1	0	0	0	0	1

Figure 5: Truth table for seven different two-input logic gates. The left column shows four different combinations of input. The output that is generated determines the behavior of the logic function.

Through the incorporation of multiple binding sites, fluorescent chemosensors can be designed to carry out logic functions. In addition to the fluorescent sensing of multiple analytes, molecular logic gates have applications such as cell-specific drug delivery, biocomputing, nanorobotics, etc.

The simplest logic gate “AND” can be created through the attachment of two receptors that quench fluorescence through PET.^[7] Whether or not either of these sites is occupied serves as a binary input. Since there is fluorescence quenching from both entities, fluorescence will not be restored unless both sites are occupied. Thus, a fluorescent chemosensor is turned into an AND logic gate that only fluoresces when both analytes are present. Many other molecular logic gates such as OR, XOR, NAND, etc. were created using different quenching mechanisms and binding site sequences.

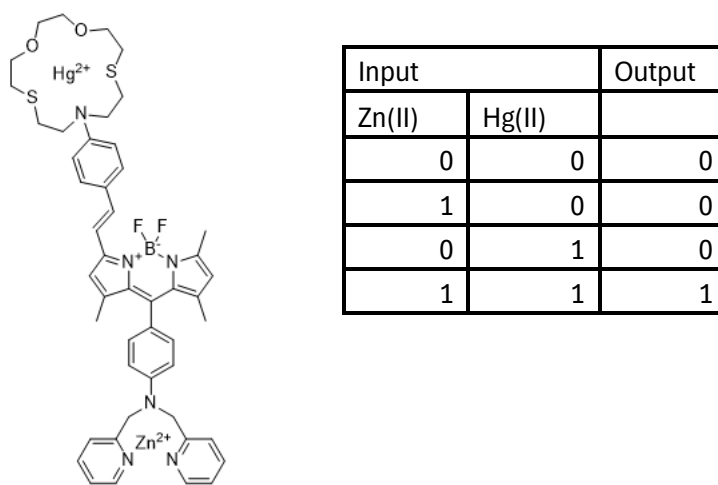


Figure 6: The two-input AND logic gate synthesized by Akkaya et al. The truth table demonstrates the AND behavior as a response is generated only when both analytes are present.^[7]

Purpose of Our Study

This study aimed to test the plausibility of applying logic gates for the tuning and manipulation of a given chemosensor's dynamic range. The idea is that for a given single-input chemosensor, the two-input version would have two equivalent receptors that both bind the same analyte. Depending on the behavior of the logic gate, the two-input chemosensor is expected to show a different dynamic range compared to the single-input chemosensor. For example, a hypothetical chemosensor built on this principle would require both binding sites to be occupied to generate a fluorescence response, while its single-input counterpart only requires one. Being an AND logic gate, the chemosensors with only a single input are not expected to generate a fluorescence response. Due to this imbalance, one would expect to see a shift and broadening in the dynamic range and an increased detection limit.

As mentioned previously, tuning of chemosensor dynamic range is a vital aspect of chemosensor development. The use of molecular logic gates provides a new approach to this problem. An advantage of this method is that it does not require the development of new ionophores with different binding affinities, since the change in dynamic range is achieved by using a known binding site multiple times.

For this purpose, we designed the following single- and two-input chemosensors and intended for the second probe to behave as a molecular AND logic gate. Naphthalimide molecules were chosen as fluorophores due to their high quantum yield, solubility, and known organic reactions. In addition, they were used in the construction of several logic gates in the past.

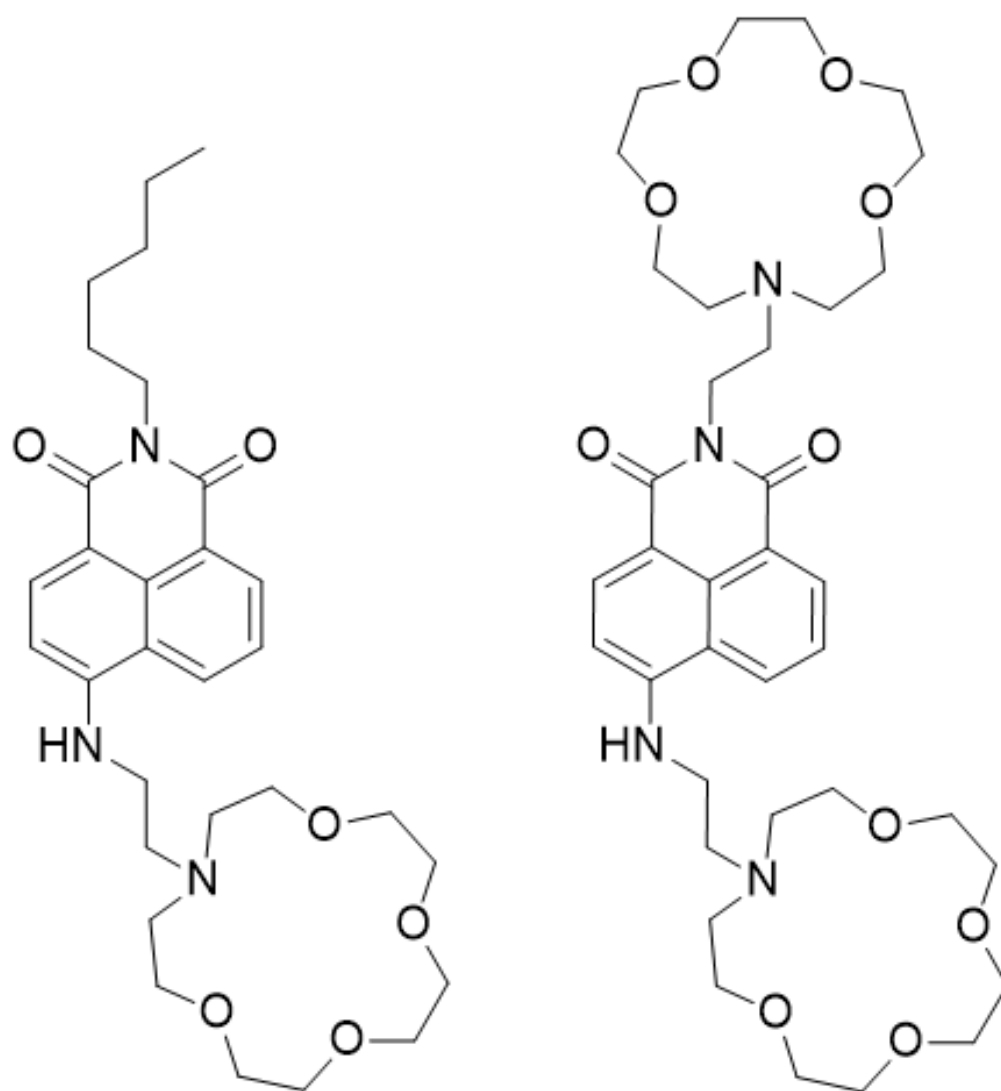
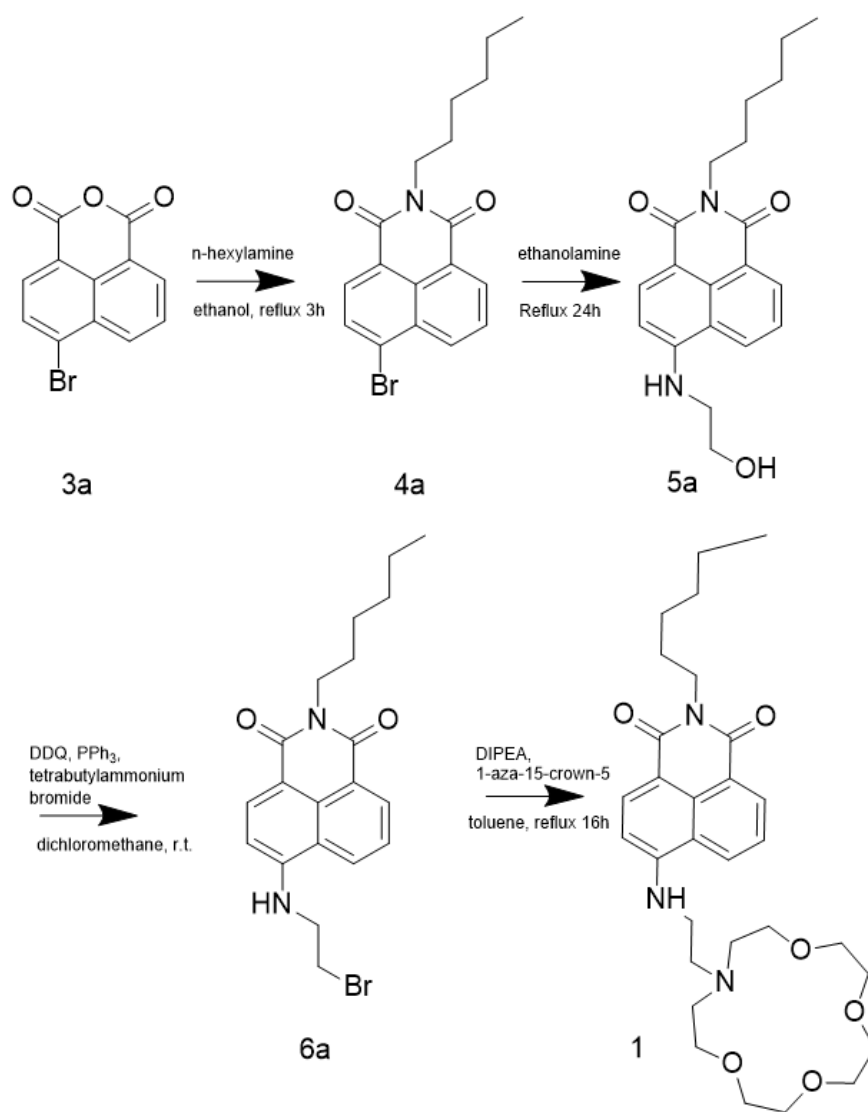


Figure 7: Na^+ chemosensors **1** and **2**.

Methods

Organic Synthesis

The general approach for sensors **1** and **2** was quite similar as shown in figure 8: attachment of a two-carbon spacer to the naphthalimide, followed by nucleophilic substitution reaction by 1-aza-15-crown-5 in the final step. Sensor **2** was also attached an ethanolamine in the imide position in addition to the 4th carbon on the naphthalene chain, which allowed for the attachment of the second crown ether. Its counterpart only has a six-carbon chain in the imide position.



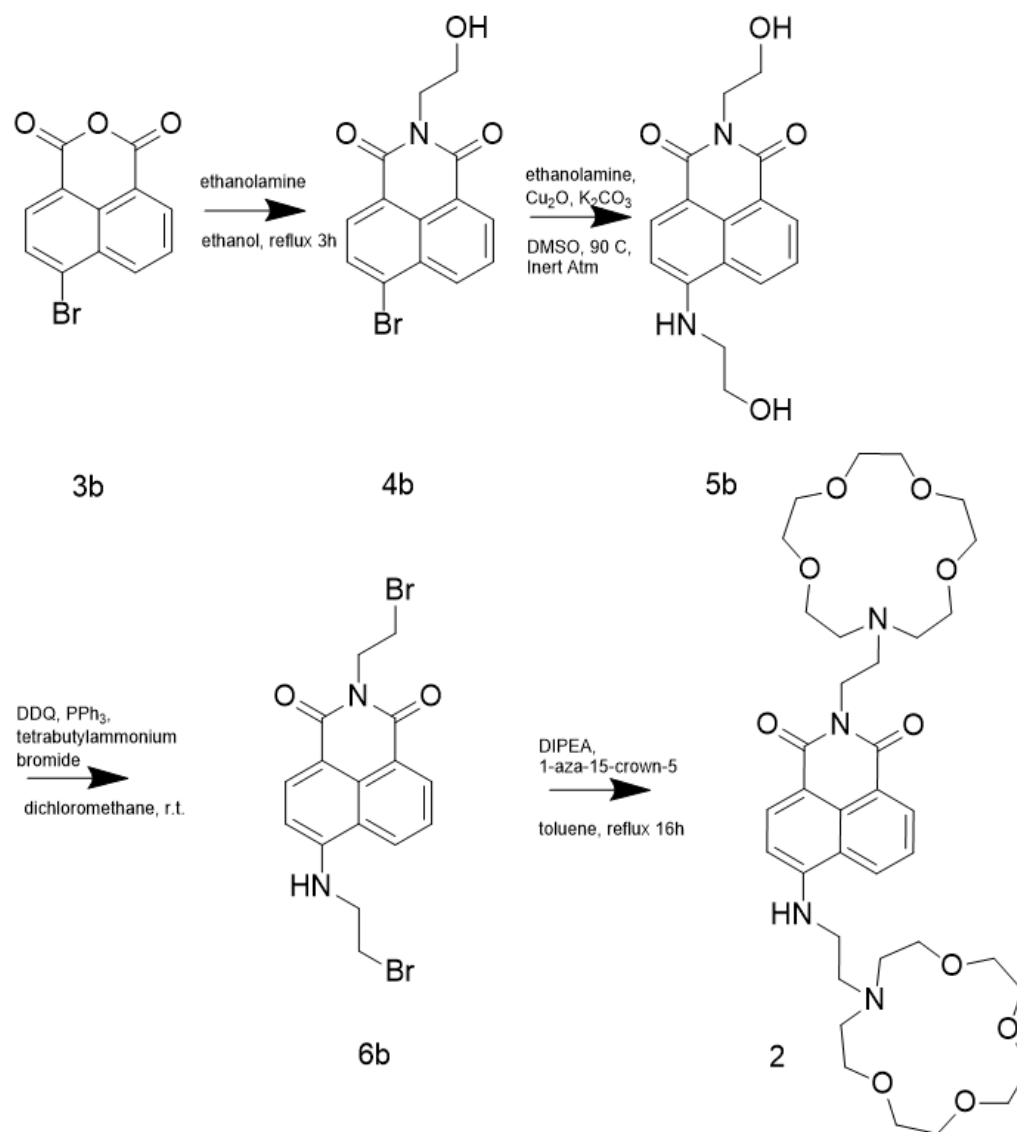
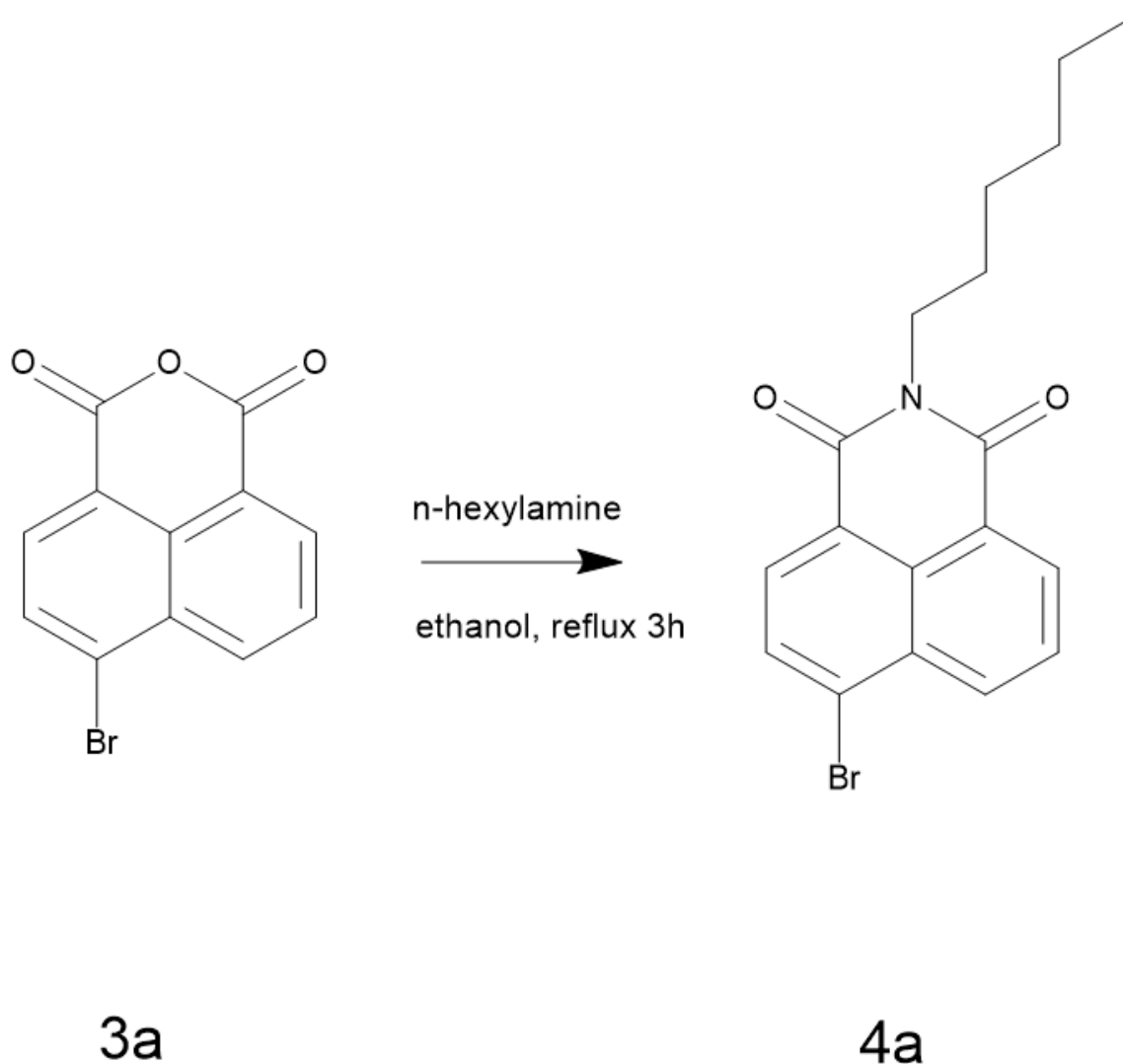
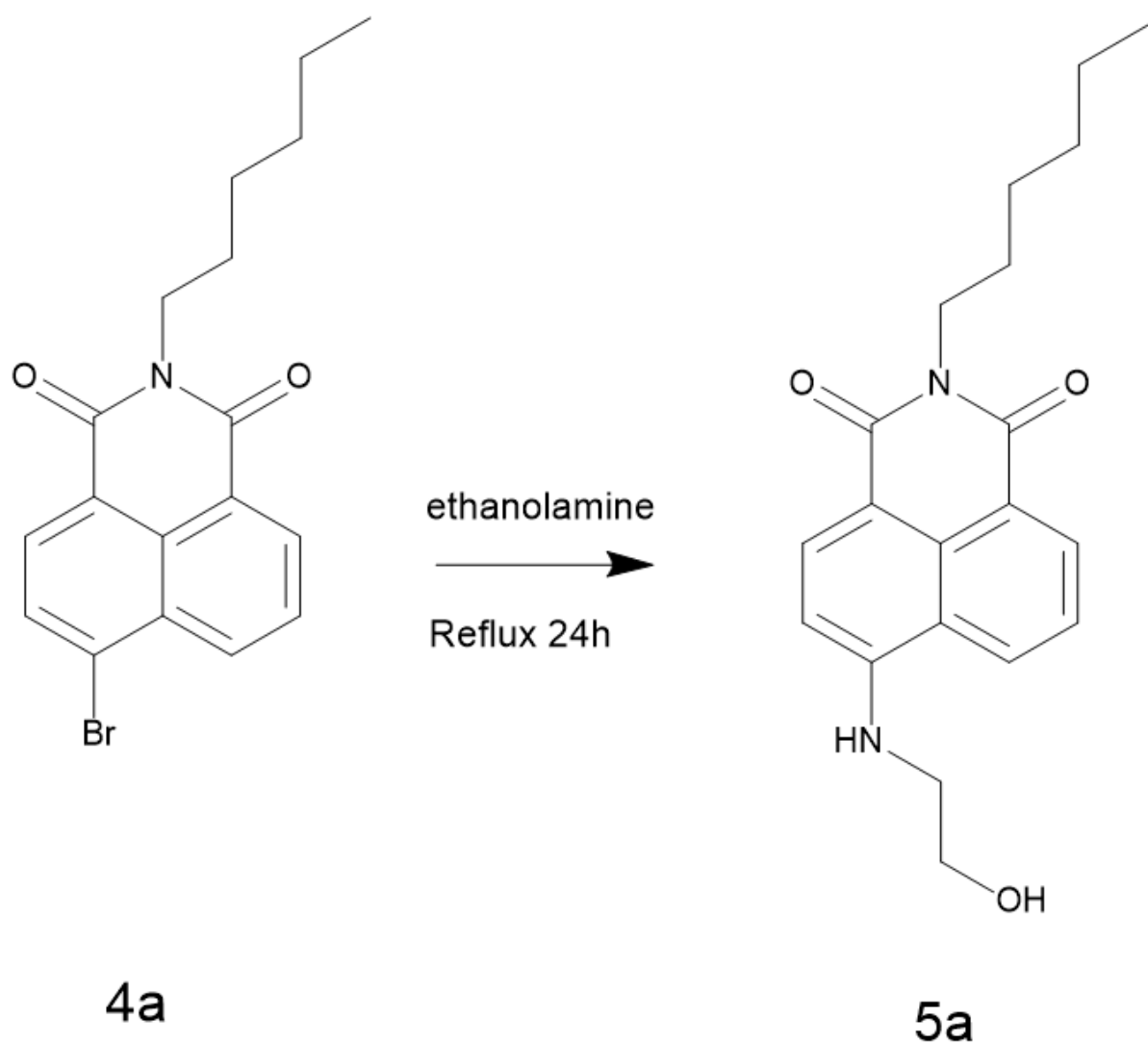


Figure 8: Synthetic pathways that were undertaken for the synthesis of **1** and **2**.

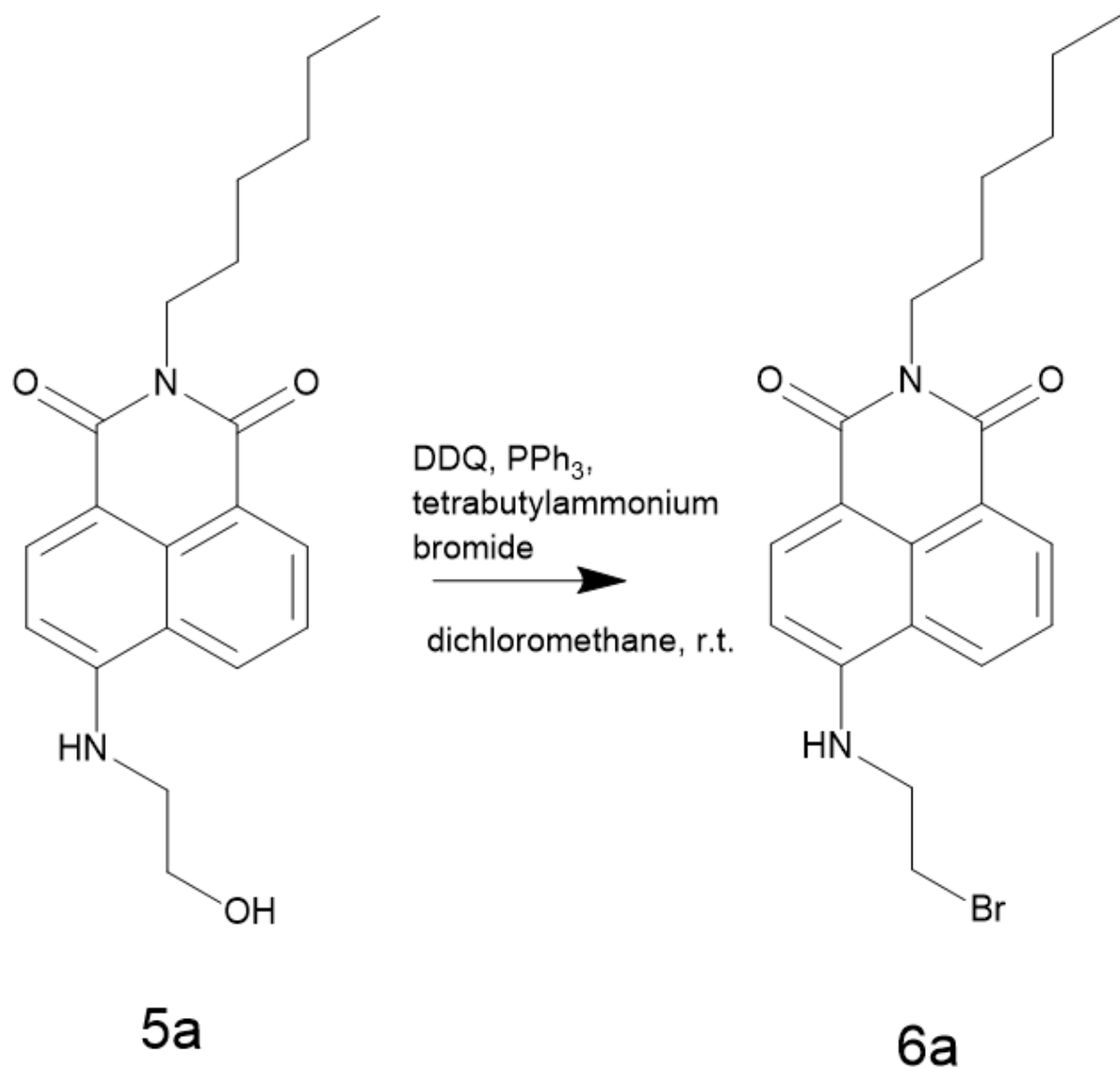
Experimental



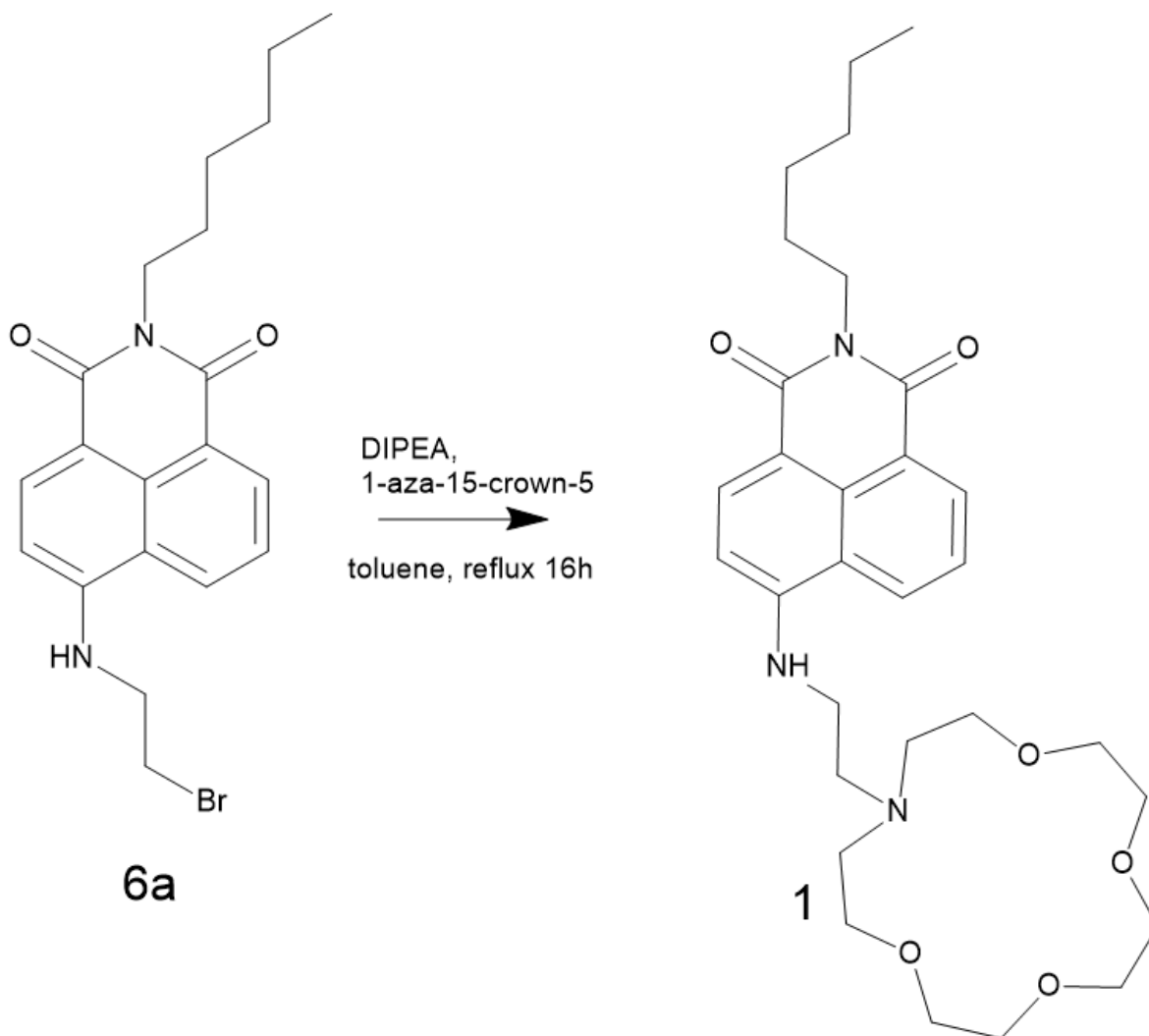
Synthesis of 4a. Anhydride **3a** (2.00g, 7.2 mmol) was dissolved in ethanol (50 mL). To this solution, 2 equivalents (1.45g, 14 mmol) of n-hexylamine was added. The solution was stirred and refluxed for 3 hours. The desired product was recrystallized from acetone overnight and filtered to obtain **4a** as a yellow precipitate (2.42 g, 6.7 mmol, 93% yield). The compound was used without further purification.^[8]



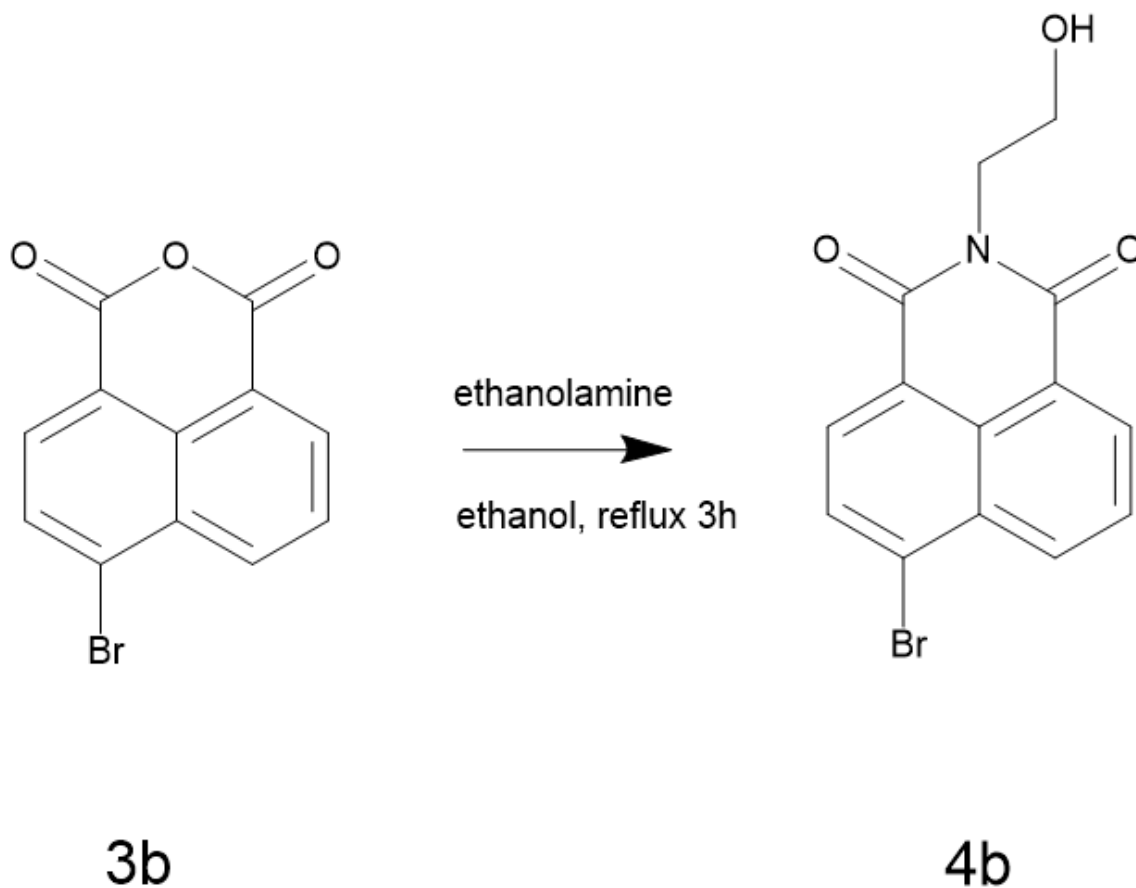
Synthesis of 5a. Naphthalimide **4a** (0.3 g, 0.83 mmol) was dissolved in ethanolamine (10 mL) and refluxed at 130 C° overnight. The reaction mixture was dissolved in DCM and washed with water twice. The organic layer was dried with MgSO₄, filtered, and dried under reduced pressure to obtain **5a** as a bright yellow solid (0.27 g, 0.79 mmol, 96% yield).



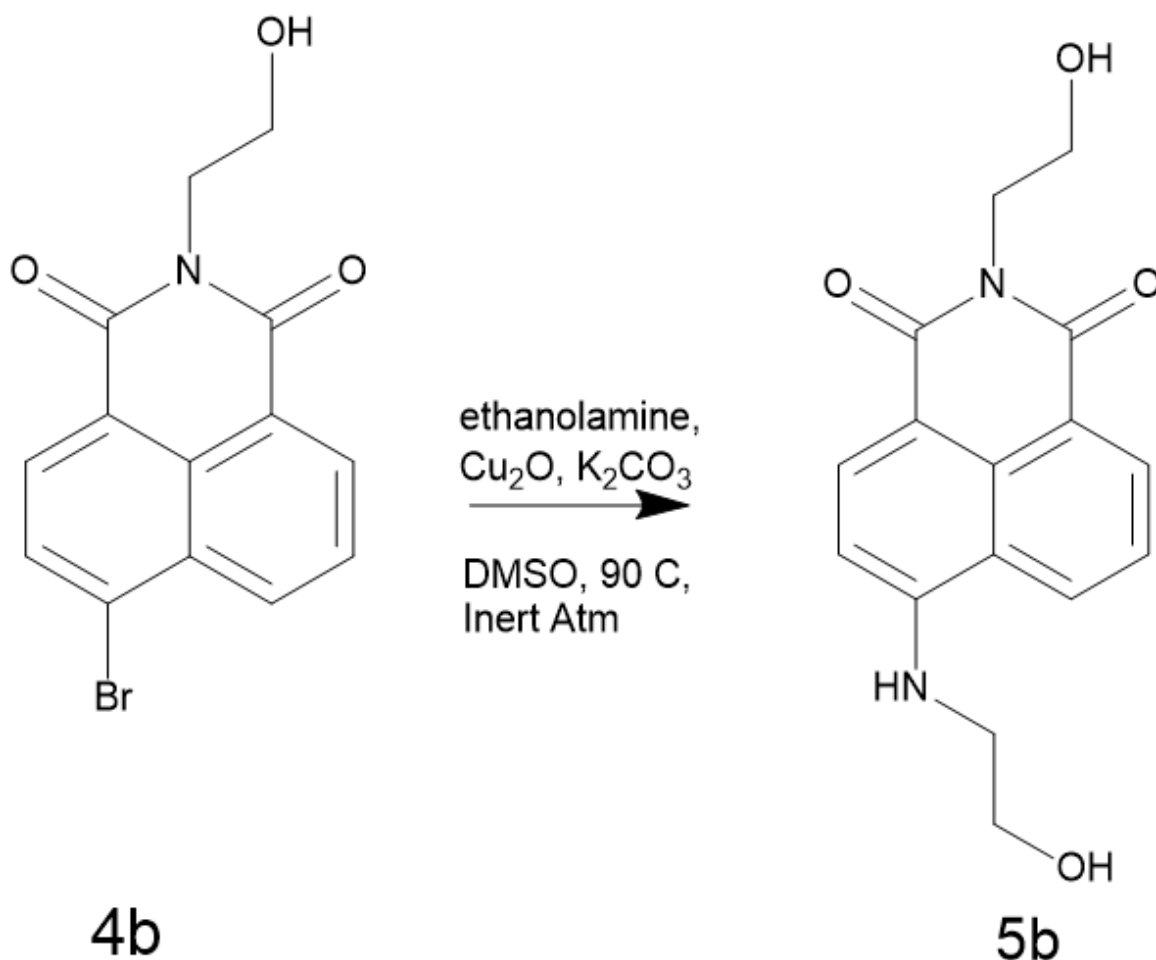
Synthesis of 6a. 1.2 equivalents of PPh₃ (0.25 g, 0.95 mmol) and DDQ (0.22 g, 0.95 mmol) were dissolved in DCM (10 mL) and stirred for 15 minutes. To this solution, 1 equivalent of **5a** (0.27 g, 0.79 mmol) was added. Finally, 1.2 equivalents of tetrabutylammonium bromide (0.31 g, 0.95 mmol) was added and the solution was stirred at room temperature overnight. The reaction mixture was concentrated in vacuo and purified through column chromatography with pure DCM as the mobile phase to obtain **6a** (0.24 g, 0.60 mmol, 72% yield).^[9]



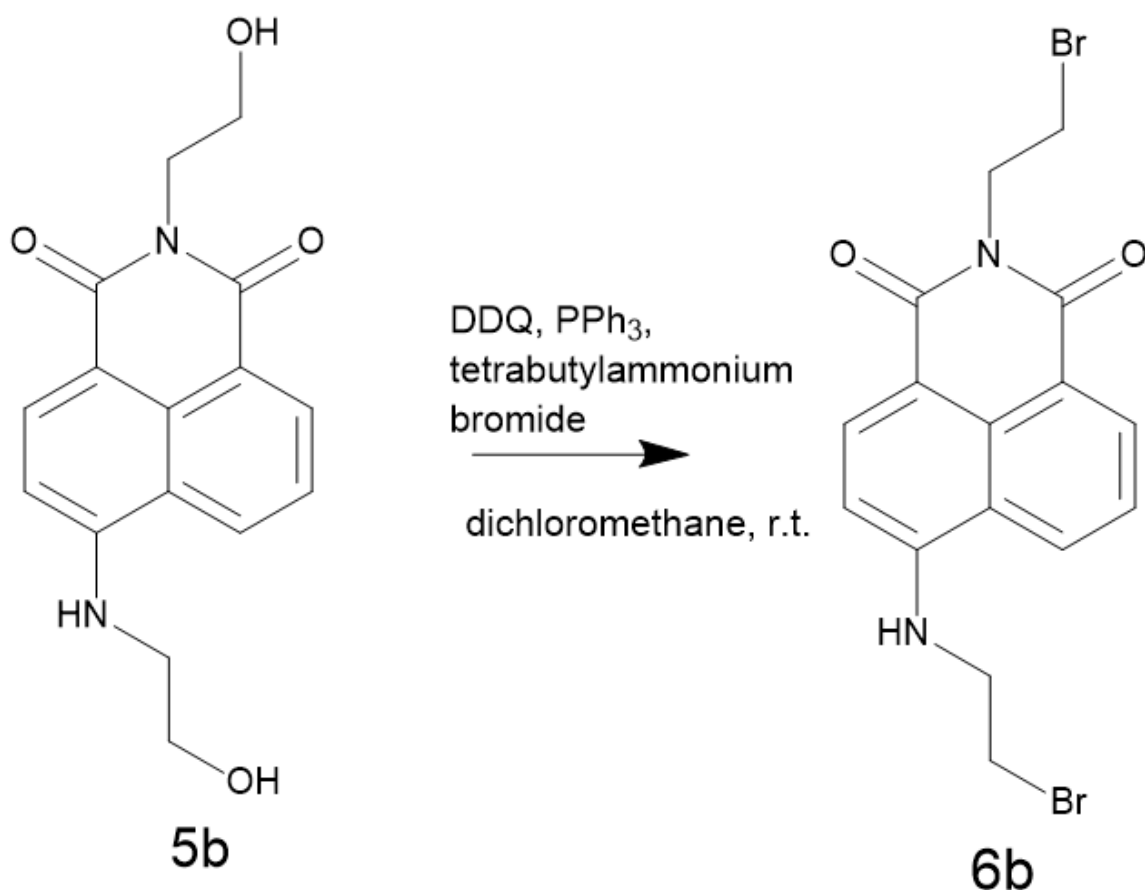
Synthesis of Chemosensor 1. 1-aza-15-crown-5 (0.015 g, 0.068 mmol) was dissolved in toluene (5 mL) and stirred under argon gas. **6a** (0.015 g, 0.045 mmol) was dissolved in toluene (5 mL) and added to the mixture. DIPEA (0.032 g, 0.23 mmol) was added, and the mixture was refluxed under argon for 16 hours. Then, the toluene was evaporated in vacuo and purified through an automated column chromatography machine (DCM:MeOH 0-10%) to obtain chemosensor **1** (0.0175 g, 0.032 mmol, 71% yield).^[10]



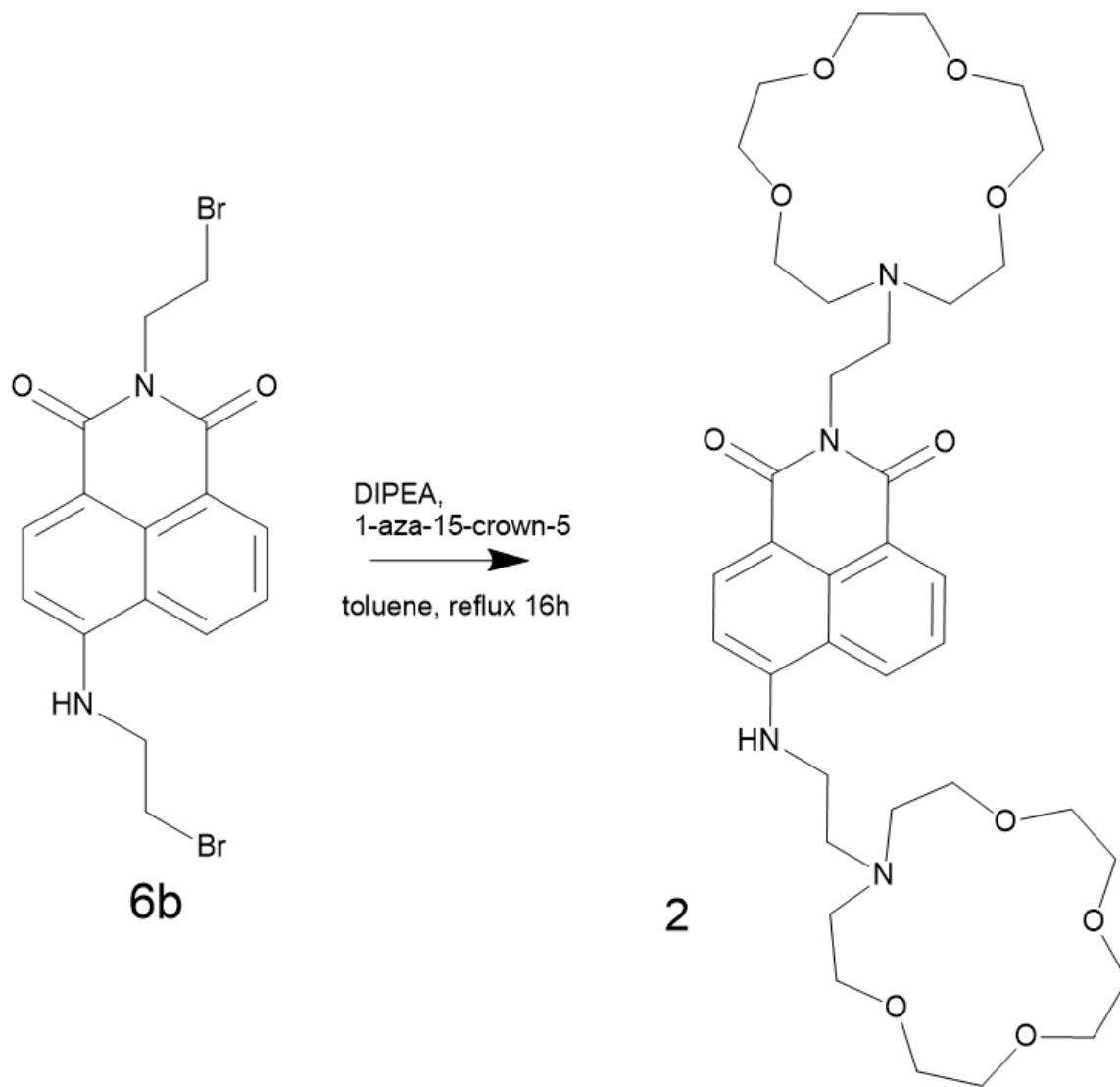
Synthesis of 4b. Anhydride **3b** (1.00 g, 3.6 mmol) was dissolved in ethanol (50 mL). Ethanolamine (0.55 mL, 4.3 mmol) was added, and the mixture was refluxed for an hour. A white precipitate emerged upon cooling, which was collected by vacuum filtration and washed with water and ethanol to obtain **4b** as a white solid (0.99 g, 3.1 mmol, 86% yield).^[11]



Synthesis of 5b. Naphthalimide **4b** (0.19 g, 0.6 mmol), Cu_2O (0.17 g, 1.2 mmol), ethanolamine (0.37 g, 6 mmol), and potassium carbonate (0.04 g, 0.3 mmol) were dissolved in DMSO (10 mL). The mixture was heated to 90 C° under argon gas overnight. After cooling to room temperature, the mixture was dissolved in DCM and washed with water three times. The organic layer was vacuum-filtered to remove some of the Cu_2O , and the filtrate was concentrated. The crude product was purified by silica gel chromatography with EtOAc:MeOH (5:1) as the mobile phase to obtain **5b** (0.13 g, 0.43 mmol, 72% yield).^[12]



Synthesis of 6b. DDQ (0.113 g, 0.5 mmol) and PPh₃ (0.131 g, 0.5 mmol) were dissolved in DCM (20 mL) and stirred at room temperature. Then, **5b** (0.030 g, 0.1 mmol) and tetrabutylammonium bromide (0.162 g, 0.5 mmol) were added. The reaction mixture was stirred at room temperature for four hours. The reaction mixture was concentrated under reduced pressure and purified by column chromatography with DCM: acetone (9:1) as the mobile phase. Fractions that showed impurities, starting material and **6b** on TLC were combined and columned again to obtain pure **6b** (0.02 g, 0.047 mmol, 47% yield).^[9]



Synthesis of Chemosensor 2. 1-aza-15-crown-5 (0.011 g, 0.046 mmol) was dissolved in toluene (10 mL) and stirred under argon gas. **6b** (0.007 g, 0.016 mmol) was added to the mixture. DIPEA (0.022 g, 0.17 mmol) was added, and the mixture was refluxed under argon for 24 hours. Then, the toluene was evaporated under reduced pressure and purified through an automated column chromatography machine. A methanol solution with a 10% triethylamine addition was prepared. This mixture was used as the polar solvent in chromatography and was added to DCM with a 0-10%

gradient. The fraction with chemosensor **2** was determined to contain triethylammonium salt by ^1H NMR. The mixture was dissolved in 50 mL of DCM and washed once with 10 mL of water to obtain chemosensor **2** (0.0012 g, 0.0017 mmol, 10% yield).^[10]

Compounds **3a-6a** and **3b-6b** are reported molecules in the literature. These molecules with the addition of naphthalimide **1** and **2** were characterized using ^1H NMR. In addition, the final products' molecular formula was confirmed with high resolution mass spectrometry (Appendix).

Spectroscopy

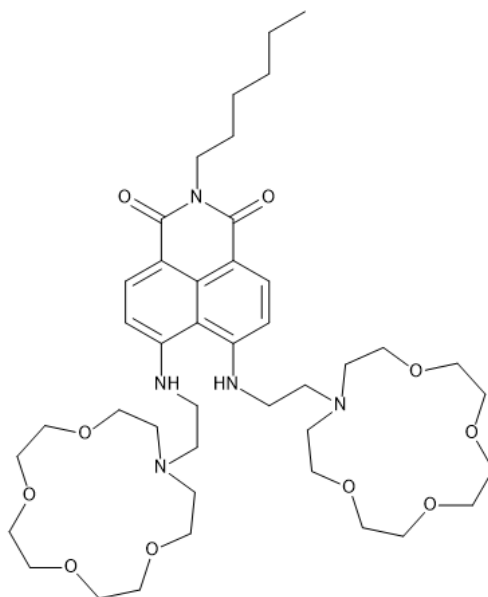
Chemosensors **1** and **2** were diluted with 50 and 25 mL of spectroscopic grade methanol respectively to obtain 0.64 and 0.068 mM solutions. 156 and 1470 microliters of these solutions were diluted to 10 mL to obtain 10 μM methanol solvents of each chemosensor. 500 mL stock solutions of NaCl in water in 1, 10, and 100 mM concentrations were prepared. Absorption and fluorescence spectroscopy experiments were carried out with an Ocean Optics Maya spectrometer.

Failed Pathways

4,5-Substituted Naphthalimide

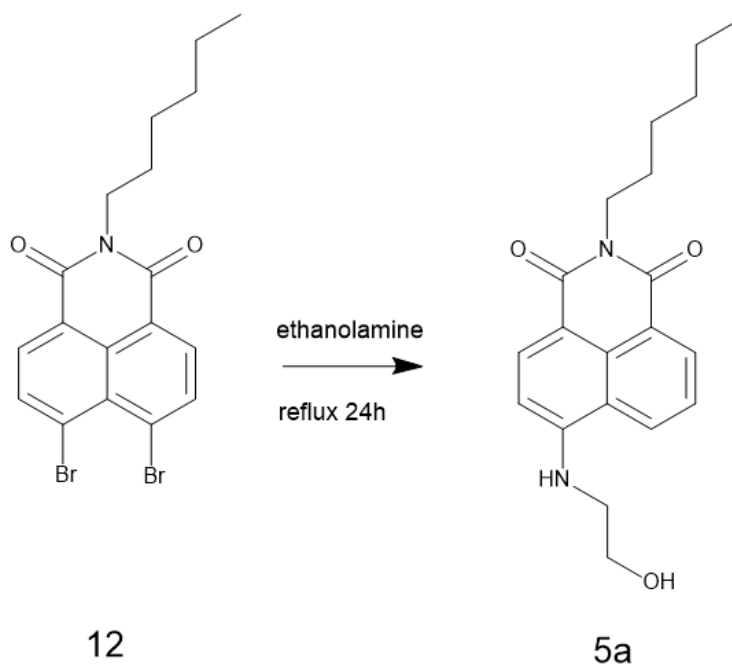
Naphthalimide **2** was not what we initially planned to synthesize. Instead, our idea was to put both binding sites on the naphthalene on carbon 4 and 5, instead of putting one on the imide and the other on the naphthalene. As compared to the final naphthalimide derivative **2**, this compound had several advantages and disadvantages.

First of all, this molecule would be expected to have identical binding sites. This is not the case when one of the imides is placed on the imide nitrogen and the other one is on the naphthalene. Binding affinity for the most part depends on the structure of the binding site itself, but regardless the two binding sites in imide **2** are electronically different. This makes it more difficult to predict whether or not the change in the dynamic range is due to a difference in binding affinities, or due to the behavior of the logic gate. Nonetheless, this is not a large concern as the binding sites on a two-input logic gate can never be fully equivalent to the binding sites on the single-input chemosensor.



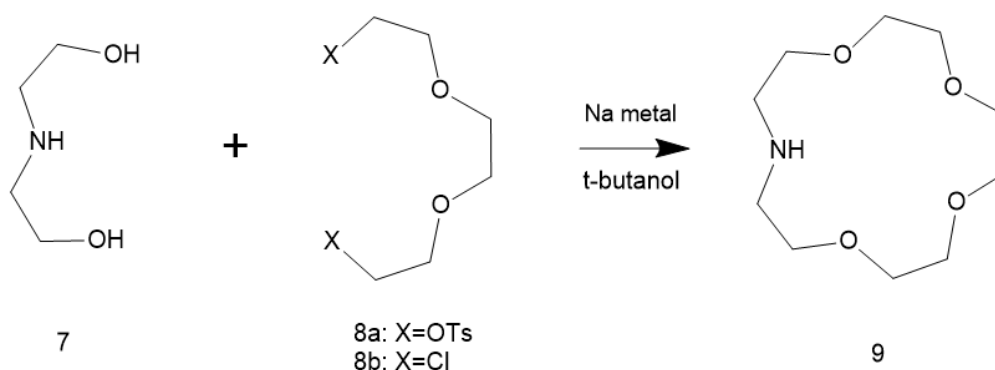
The problem with putting the crown ethers on the 4th and 5th position is that they might be too sterically hindered. This poses problems with regard to both organic syntheses, and their binding affinity towards sodium ions. Due to steric hindrance, binding of the second sodium might be much more unfavorable compared with the first binding, therefore leading to an extension in the dynamic range that is not due to the logic gate.

We also faced a synthetic challenge on the third step that we could not explain. This step is almost identical to the synthesis of **5a**, except with the aromatic substitution of two bromines. This reaction was tried with identical conditions to the synthesis of **5a**, and with procedures from the literature. The reported procedure was quite similar to our purposes except for the use of chlorine instead of bromines on positions 4 and 5. The reactions we ran inexplicably performed the nucleophilic aromatic substitution with ethanolamine on the 4th position and reduced the 5th position. The NMR spectrum of this product matched that of **5a**.



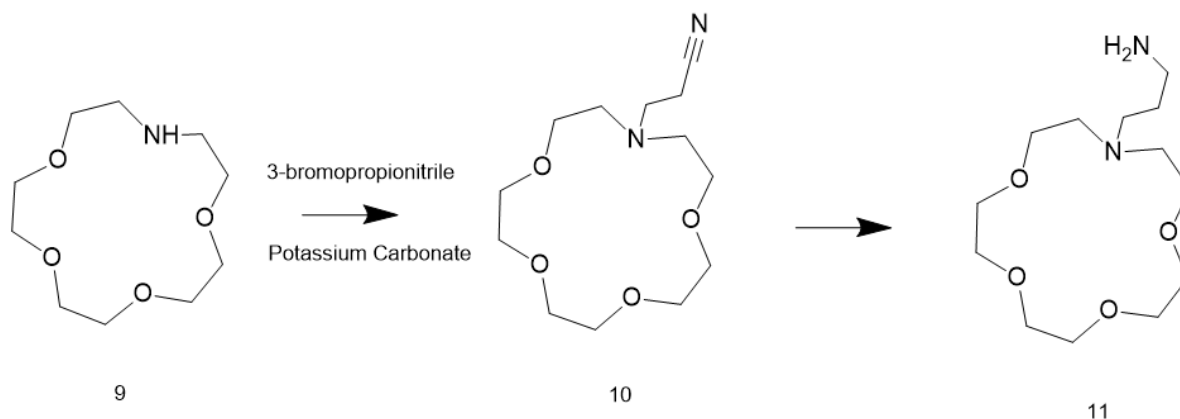
1-Aza-15-Crown-5

We initially attempted to synthesize our reactive aza-crown due to its cost. Later, we decided to buy a small amount of the crown when its preparation proved elusive. Two different triethylene derivatives were used for this purpose with two different leaving groups: chlorides and tosylates. No reaction was observed between chlorinated triethylene glycol and diethanolamine, despite high reported yields in the literature. The chlorinated starting material, which was shown to be less reactive in the same article, did form 1-aza-15-crown-5 with more than a 50% yield. The problem with this was the elimination of starting material **8b**. The structures of the aza-crown and the byproduct were determined by ^1H NMR. However, we found the purification of this mixture to be too difficult, as crown ethers are not suitable for silica gel column chromatography.



Extension of the Crown with a Spacer

We performed reactions between the aza-crown and a three-carbon nitrile molecule. The intent was to reduce the nitrile to a primary amine and do a nucleophilic aromatic substitution with the naphthalimide derivative.



The main issue with this convergent approach is that the crown ether-containing molecule requires multiple purification processes, which is quite impractical as mentioned. The second problem is that the final step in this process is not trivial due to the problems we faced with the 4,5-disubstituted naphthalimide **12**. The synthetic pathway we used instead has a very simple nucleophilic substitution of a bromine by the aza-crown, which makes the pathway much more reliable and minimizes the number of purification steps that the crown ether needs to go through.

Results

Absorption Spectroscopy

Measurements were taken as an average of 25 scans, each taking 160 milliseconds on the Ocean Maya spectrophotometer with a charge-coupled detector. For naphthalimides **1** and **2**, three different samples were measured: dark, blank, and the chemosensor itself. The transmittance was measured for the three samples between 200 and 1100 nanometers, and the data was plugged into Beer-Lambert's law in order to obtain absorbance. I_0 and I in this instance are obtained by subtracting the dark measurement from the blank and chemosensor sample to account for background noise.

$$A = \log_{10} \left(\frac{I_0}{I} \right) = \epsilon cl$$

Naphthalimide **1** was found to absorb light in the 360-480 nm range with the absorption maximum at 431 nanometers. Naphthalimide **2** absorbs in roughly the same range with the absorption maximum at 427 nanometers. The molar absorptivity (ϵ) was calculated as $12600 \text{ M}^{-1}\text{cm}^{-1}$ and $10700 \text{ M}^{-1}\text{cm}^{-1}$ for chemosensors **1** and **2** respectively.

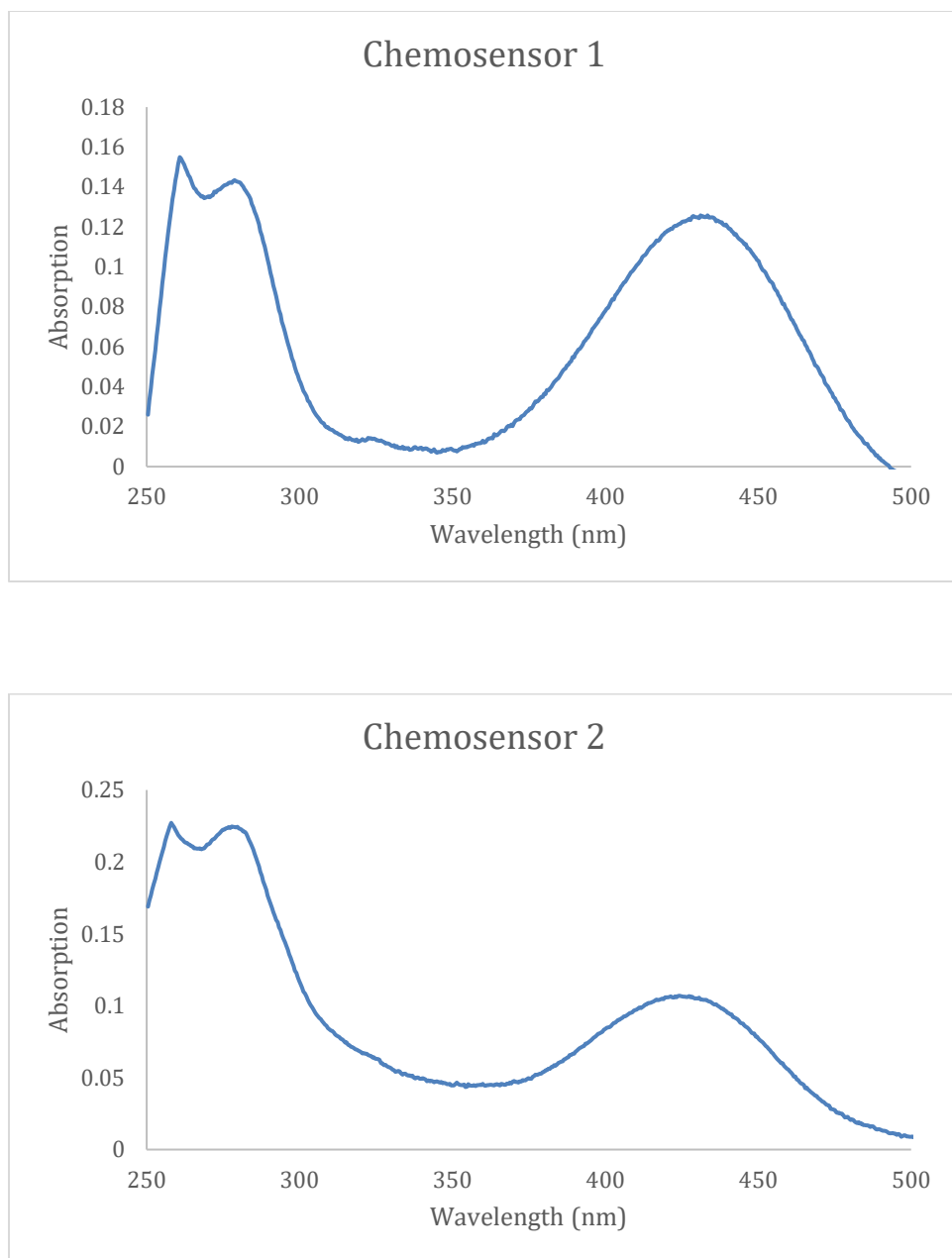


Figure 9: Absorption spectra for naphthalimide derivatives **1** and **2**.

Fluorescence Spectroscopy

With consideration of the absorption spectra, 455 nm was selected as the excitation wavelength for the fluorimetry experiments. 10 scans were averaged for each measurement with an integration time of 400 ms. Dark scans were taken for each experiment to account for background noise.

In the absence of Na⁺ ions in solution, fluorescence intensity for chemosensor **1** was measured to be 1.24 times more fluorescent compared with chemosensor **2** in arbitrary units. Chemosensor **1** was titrated with a 100 mM solution of NaCl in water until saturation was reached around a concentration of 6 mM NaCl. At the saturation point, a 4.2-fold increase in fluorescence was observed. Dilution was accounted for when calculating the Na⁺ concentration in the cuvette. Titration with the 1 mM aliquot led to an observable change in fluorescence intensity but did not saturate the probe.

We attempted to titrate the chemosensor **2** with the 1 mM aliquot, but no significant increase in fluorescence was observed. The titration experiment involving 10 mM additions led to some increase in fluorescence but did not reach saturation. We were finally able to titrate the second chemosensor using 100 mM additions. Fluorescence intensity was measured at 23388 in the absence of Na⁺, compared to 29038 for chemosensor **1**. These values are given in arbitrary units but can act as a measure of comparative fluorescence. The lower fluorescence intensity compared with the first chemosensor can be explained by the fact that chemosensor **2** experiences PET from two aza-crown ethers as compared to a single one. Saturation was reached approximately at 15 mM, with a 3.6-fold increase in fluorescence intensity.

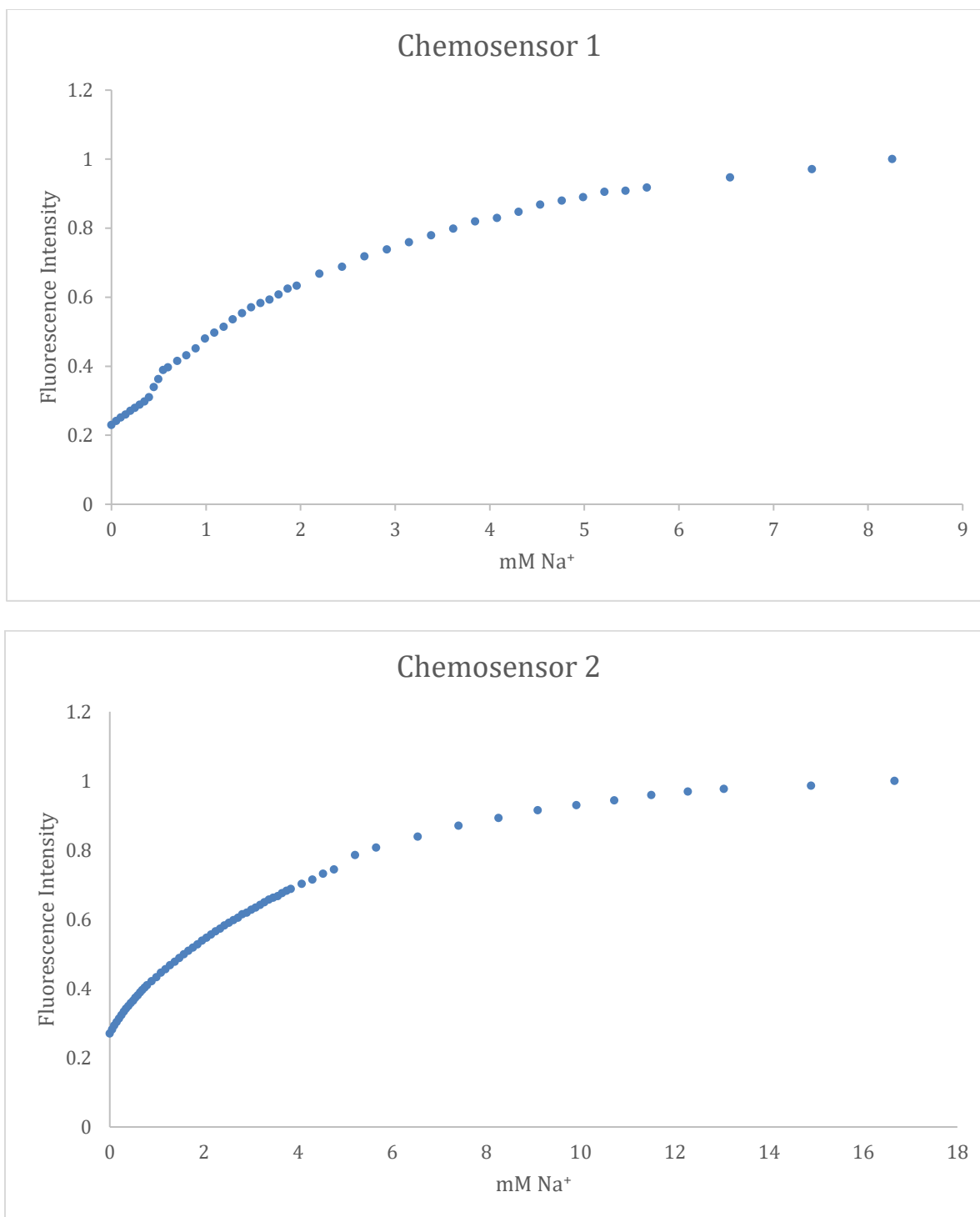


Figure 10: Fluorescence titration experiments for chemosensors **1** and **2**.

Binding Constant

A non-linear line of best fit was found for both titration curves using the least squares method. After normalizing fluorescence intensity, a hyperbolic curve was plotted using the following equation. This equation was derived by relating the measurable change in fluorescence to the fraction of naphthalimide with a bound Na⁺ ion.

$$K = \frac{[C \cdot A]}{[C][A]}$$

$$\text{Bound Fraction} = \frac{Fl - Fl_0}{Fl_{max} - Fl_0} = \frac{[C \cdot A]}{[C] + [C \cdot A]}$$

$$\frac{[C \cdot A]}{[C] + [C \cdot A]} \times \frac{1}{\frac{1}{[C]}} = \frac{\frac{[C \cdot A]}{[C]}}{\frac{[C \cdot A]}{[C]} + 1} = \frac{K \times [A]}{1 + K \times [A]}$$

We can rearrange the above equation to isolate measured fluorescence on the left side of the equation.

$$Fl = \frac{(Fl_{max} - Fl_0) \times K \times [A]}{1 + K \times [A]} + Fl_0$$

The free analyte concentration $[A]$ is the unknown in this equation. The known Na^+ addition is equal to $[A]+[C\cdot A]$, but we can approximate that $x\sim[A]$, since the chemosensor concentration $[C]$ is three orders of magnitude smaller than $[A]$.

Fl : Fluorescence intensity at a given point

Fl_{max} : Fluorescence at the saturation point

Fl₀ : Fluorescence in the absence of Na^+ ions

[C] : Free chemosensor concentration

[A] : Free Na^+ concentration

[C • A] : Concentration of chemosensor that is bound to analyte

K : Binding constant in mM^{-1}

x : Concentration of added Na^+ in mM

The given constants Fl_{max} and Fl_0 are known experimentally, while x is the variable that is the added sodium concentration upon which the fluorescence intensity (Fl) depends. However, we later realized that the highest fluorescence intensity that we measured does not reflect the asymptote of the titration curve. So, we also used the solver tool to generate a Fl_{max} value. Using these constants, variables, and the known titration curve, a line of best fit can be generated to determine the binding constant (k). After plugging in the known constants for every concentration point in Excel, a value for the binding constant was guessed to generate a temporary hyperbolic curve. The points on

these curves were subtracted from the measured values and squared. The squared values were summed. Using the solver tool in excel, the sum of squares value was minimized by altering the value for the binding constant. This process revealed the binding constant for the chemosensor **1** to be 0.33 mM^{-1} .

This process was more difficult for chemosensor **2**, as the two binding sites cannot be titrated in isolation. There are kinetic models used to determine the binding constant when multiple receptors are present; however, the use of such models requires insight on how the fluorescence intensity changes when only a single analyte is bound. If chemosensor **2** behaves as an ideal AND logic gate, the increase in fluorescence intensity is only due to the $[\text{Chemosensor} \cdot 2\text{Na}^+]$ complex. Although, molecular logic gates are not always completely binary, as the binding of a single ion can generate a small fluorescence response in an AND logic gate.^[7]

When the equation above was fitted into the second titration curve, k was determined to be 0.19 mM^{-1} from the least squares fit method. This number can be treated as the composite binding constant for the chemosensor, as it is not a measure of the binding constant of either binding site. However, this number is still useful since the equation and the k value can be used to calculate the Na^+ concentration from a fluorescence measurement.

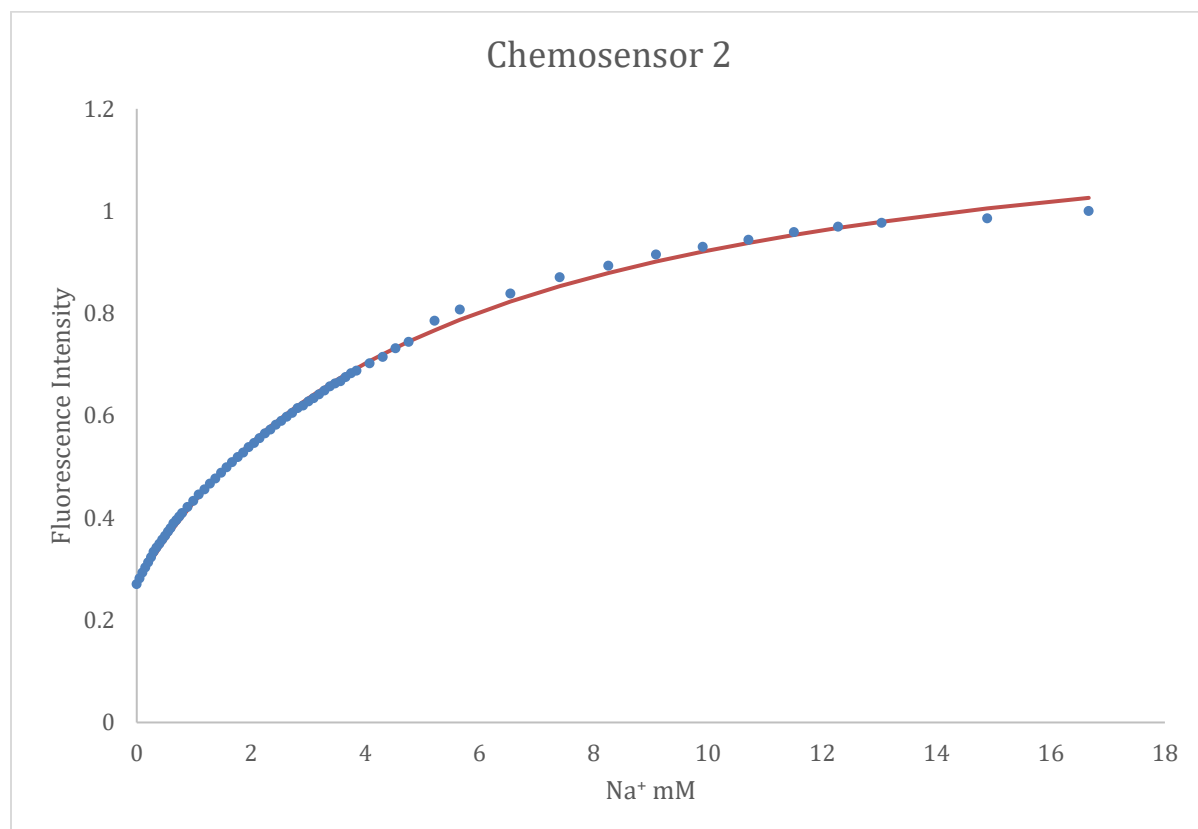
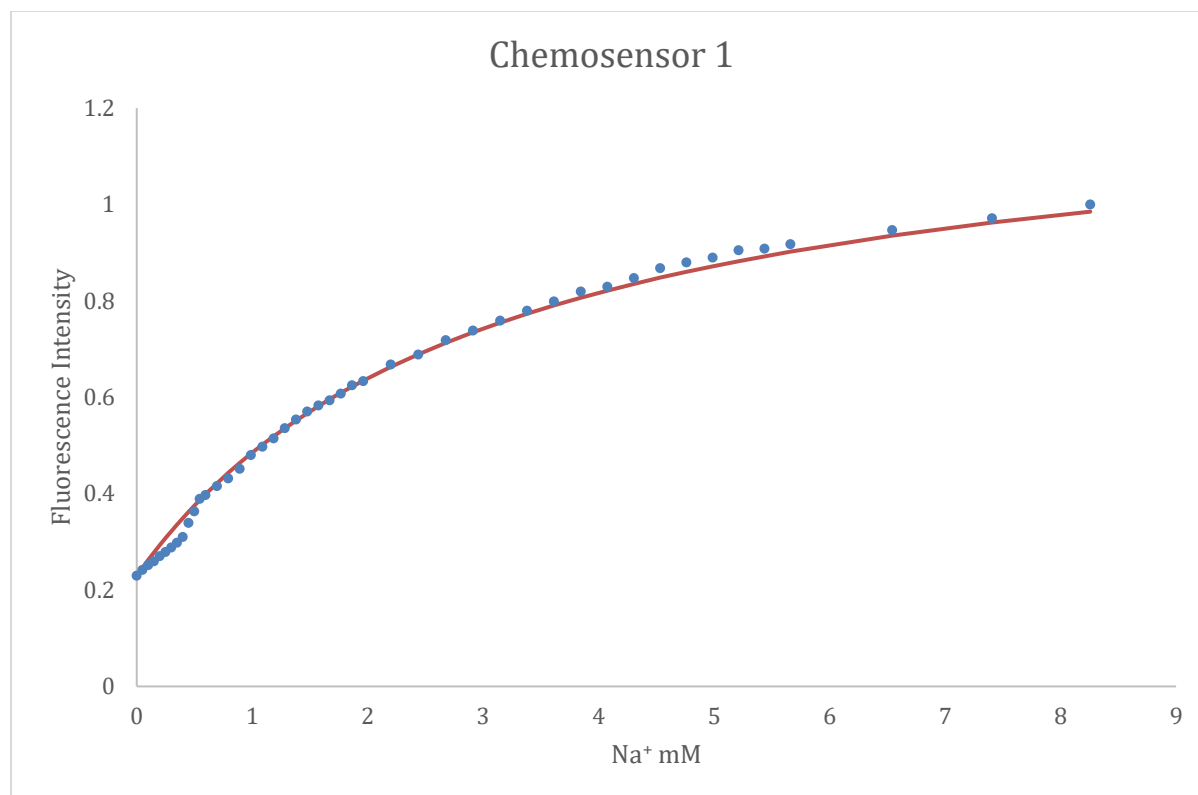


Figure 11: The titration data with a line of best fit.

Detection Limit

The detection limit is the lowest concentration of the analyte that is sufficient to generate a signal that is distinguishable from background noise. Due to the dependence on noise, the detection limit may depend on the precision of instruments. Usually, the detection limit is taken as $(3 \cdot \text{SD of noise}) / (\text{binding constant})$. The standard deviation of the noise was calculated in excel from the dark scans, and the binding constants are known from line fitting method. This calculation revealed the detection limit to be 0.0018 mM and 0.0043 mM for chemosensors **1** and **2**, respectively. As hypothesized, the detection limit is higher for the AND logic gate. This is because a single molecule of chemosensor **2** requires two Na^+ ions for every single ion required by chemosensor **1**.

$$3\sigma/k$$

Conclusions

Interpretation of Results

We were able to increase the detection limit and saturation point of a chemosensor through the incorporation of an AND logic gate. In addition to this increase, a broader dynamic range was observed for the second chemosensor. All in all, we were able to implement a new method of altering chemosensor dynamic range, while also discovering a useful field of application for molecular logic gates. Tuning of chemosensor dynamic range is a problem that is traditionally solved through the development of receptors with different binding affinities towards the analyte.

Limitations

Chemosensor **2** was designed to behave as an AND logic gate. The problem is that the nature of the logic function cannot be determined definitively. This is due to the fact that both binding sites require the same input: Na^+ . For traditional logic gates, the nature of a chemosensor is understood by trying all four input combinations: absence of both, inclusion of one input or the other, or inclusion of both. These trials are not possible to perform for chemosensor **2** as the occupation of only a single site cannot be controlled. Both inputs (Na^+) are always present in the solution. The only way of inferring the logic function is through the dynamic range. For an AND gate a broadening is expected for the dynamic range, since one of the binding sites needs to be occupied before the second ion can turn on fluorescence.

Another limitation of the second chemosensor is that the two binding sites that make up the AND logic gate are not chemically equivalent to one another, as the two azacrowns are attached to the naphthalene and the imide. Even though binding affinity relies mostly on the structure of the binding site, the mode of attachment can have certain effects on the binding affinity. The central idea of this study can be further investigated by testing the concept on a symmetrical AND logic gate where both ionophores are equivalent. This might give rise to more predictive power when determining how much the dynamic range will change compared with the single input chemosensor. As mentioned in the failed pathways section, the incorporation of two equivalent binding sites to a naphthalimide was not feasible.

The final limitation is the difficulty of purifying a chemosensor with two binding sites on it with silica gel column chromatography.

Future Research

In this study we demonstrated how an AND logic gate can be used to change the dynamic range of a chemosensor. For two inputs, 16 different logic gates are possible, and some of these were successfully implemented in molecules. Future research can reveal how more unusual logic gates can influence the fluorescence response curves of chemosensors.

For example, a hypothetical XOR gate that detects a single analyte will have a response curve that initially increases in fluorescence intensity, and gradually decreases after peaking. This is because an output is generated exclusively when one or the other

site is occupied. No response is generated when neither or both sites are occupied.

Conversely, the hypothetical NXOR logic gate will behave completely opposite compared with XOR. This logic gate would display an output when neither or both sites are occupied, but not when only a single site is occupied (Figure 5).

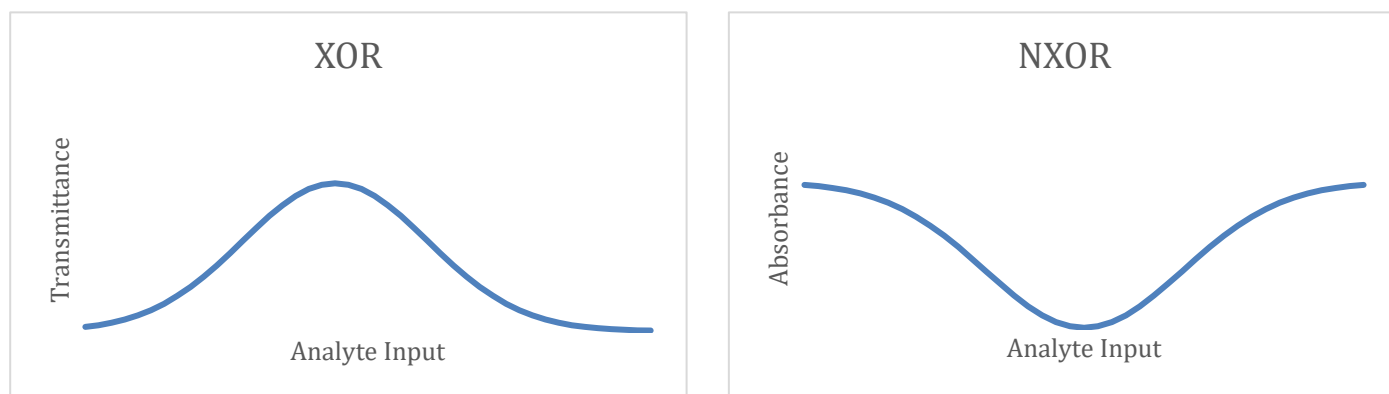


Figure12: Hypothesized behavior of different molecular logic gates. XOR responds only when a single site is occupied, while NXOR generates a response when neither or both sites are occupied.

These hypothetical logic gates are not as useful as an AND logic gate. We were able to use the AND logic gate to increase the detection maximum of chemosensors; it is unclear whether or not different logic gates will have practical uses. In either case, future research can reveal the behavior of such logic gates.

References

- (1) Harris, D. C.; Lucy, C. A. *Quantitative Chemical Analysis*; New York, Ny W. H. Freeman And Company, **2016**.
- (2) Withe, C. E.; Argauer, R. J. *Fluorescence Analysis*; **1970**.
- (3) Wu, Di, et al. “Fluorescent Chemosensors: The Past, Present and Future.” *Chemical Society Reviews*, vol. 46, no. 23, **2017**, pp. 7105–7123, <https://doi.org/10.1039/c7cs00240h>.
- (4) Li, Xiaohua, et al. “Design Strategies for Water-Soluble Small Molecular Chromogenic and Fluorogenic Probes.” *Chemical Reviews*, 114, **2013**, pp. 590–659, <https://doi.org/10.1021/cr300508p>.
- (5) Minta, A, and R Y Tsien. “Fluorescent Indicators for Cytosolic Sodium.” *Journal of Biological Chemistry*, vol. 264, no. 32, Nov. **1989**, pp. 19449–19457, [https://doi.org/10.1016/s0021-9258\(19\)47321-3](https://doi.org/10.1016/s0021-9258(19)47321-3).
- (6) Akkaya, Engin U., et al. “Molecular Logic Gates: The Past, Present and Future.” *Chemical Society Reviews*, 47, **2018**, pp. 2228–2248, <https://doi.org/10.1039/c7cs00491e>.
- (7) Akkaya, Engin U., et al. “Selective Manipulation of ICT and PET Processes in Styryl-Bodipy Derivatives: Applications in Molecular Logic and Fluorescence Sensing of Metal Ions.” *Journal of the American Chemical Society*, vol. 132, no. 23, 18 Mar. **2010**, pp. 8029–8036, <https://doi.org/10.1021/ja1008163>. Accessed 18 Jan. 2023.
- (8) Wu, Y.; Xu, J.; Hu, Y.; Bi, S.; Wu, S.; Wang, L. Micellization of 4-Hydroxynaphthalimides: The Solvent-Induced Aggregation and the Detection of Low-Level Water in THF. *Chemistry Letters* **2016**, 45 (10), 1162–1164. <https://doi.org/10.1246/cl.160477>.

- (9) Wang, X.; Chen, Z.; Tong, L.; Tan, S.; Zhou, W.; Peng, T.; Han, K.; Ding, J.; Xie, H.; Xu, Y. Naphthalimides Exhibit in Vitro Antiproliferative and Antiangiogenic Activities by Inhibiting Both Topoisomerase II (Topo II) and Receptor Tyrosine Kinases (RTKs). *European Journal of Medicinal Chemistry* **2013**, *65*, 477–486.
<https://doi.org/10.1016/j.ejmech.2013.05.002>.
- (10) Ravi, A.; P. Sivarama Krishnarao; Shumilova, T. A.; Khrustalev, V. N.; Ruffer, T.; Lang, H.; Kataev, E. A. Cation Molecular Exchanger Based on a Conformational Hinge. *Organic Letters* **2018**, *20* (19), 6211–6214.
<https://doi.org/10.1021/acs.orglett.8b02687>.
- (11) Zhou, J., Liu, H., Jin, B., Liu, X., Fu, H., Shangguan, D. A guanidine derivative of naphthalimide with excited-state deprotonation coupled intramolecular charge transfer properties and its application. *Journal of Materials Chemistry* **2013**, *C*, 1(29), 4427.
<https://doi.org/10.1039/c3tc30853g>
- (12) Fang, C.; Zhou, J.; Liu, X.; Cao, Z.; Di-hua Shangguan. Mercury(Ii)-Mediated Formation of Imide-Hg-Imide Complexes. *Dalton Transactions* **2011**, *40* (4), 899–903.
<https://doi.org/10.1039/c0dt01118e>.
- (13) J.P. Desvergne; Czarnik, A. W. Chemosensors of Ion and Molecule Recognition; Springer Science & Business Media, 2012.
- (14) Dong, H.-Q.; Wei, T.-B.; Ma, X.-Q.; Yang, Q.-Y.; Zhang, Y.-F.; Sun, Y.-J.; Shi, B.-B.; Yao, H.; Zhang, Y.-M.; Lin, Q. 1,8-Naphthalimide-Based Fluorescent Chemosensors: Recent Advances and Perspectives. *Journal of Materials Chemistry C* **2020**, *8* (39), 13501–13529. <https://doi.org/10.1039/d0tc03681a>.

- (15) Spiteri, J. C.; Johnson, A. D.; Denisov, S. A.; Gediminas Jonusauskas; McClenaghan, N. D.; Magri, D. C. A Fluorescent and Logic Gate Based on a Ferrocene-Naphthalimide-Piperazine Format Responsive to Acidity and Oxidizability. *Dyes and pigments* 2018, 157, 278–283.
<https://doi.org/10.1016/j.dyepig.2018.04.060>.

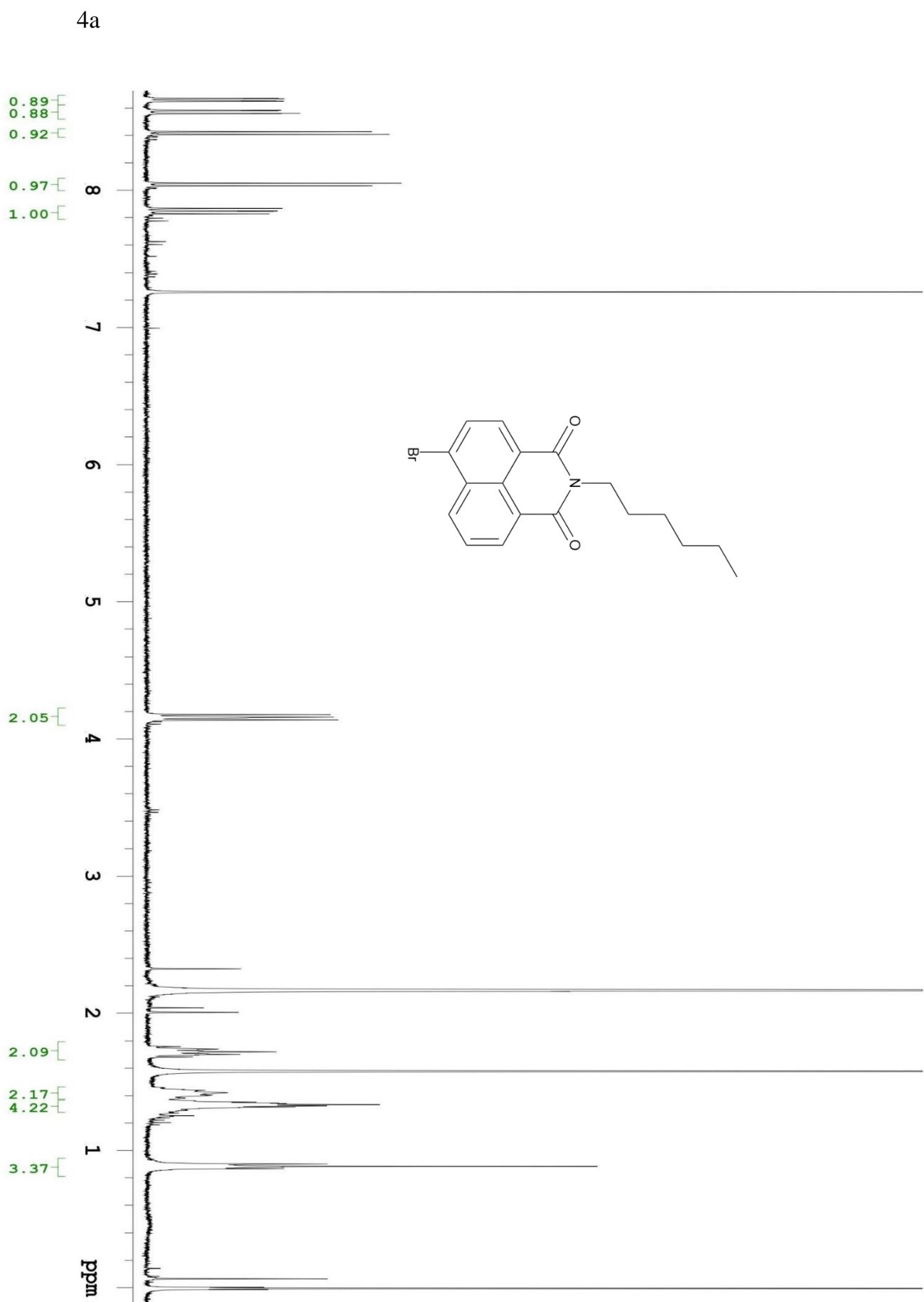
Images

- (16) *Jablonski diagram of absorbance, non-radiative decay, and fluorescence*. Wikimedia Commons.
https://commons.wikimedia.org/wiki/File:Jablonski_Diagram_of_Fluorescence_Only-ru.svg (accessed 2024-04-12).
- (17) *File:Stokes shift- Rh6G.png - Wikipedia*. commons.wikimedia.org.
https://en.wikipedia.org/wiki/File:Stokes_shift-_Rh6G.png (accessed 2024-04-12).
- (18) Prabowo, B. A.; Cabral, P. D.; Freitas, P.; Fernandes, E. The Challenges of Developing Biosensors for Clinical Assessment: A Review. *Chemosensors* 2021, 9 (11), 299. <https://doi.org/10.3390/chemosensors9110299>.

Figure 4 was reproduced with permission from the author. The remaining images are in the public domain.

Appendix

The ^1H NMR spectra for all intermediates and final chemosensors. The mass spectra are also depicted.



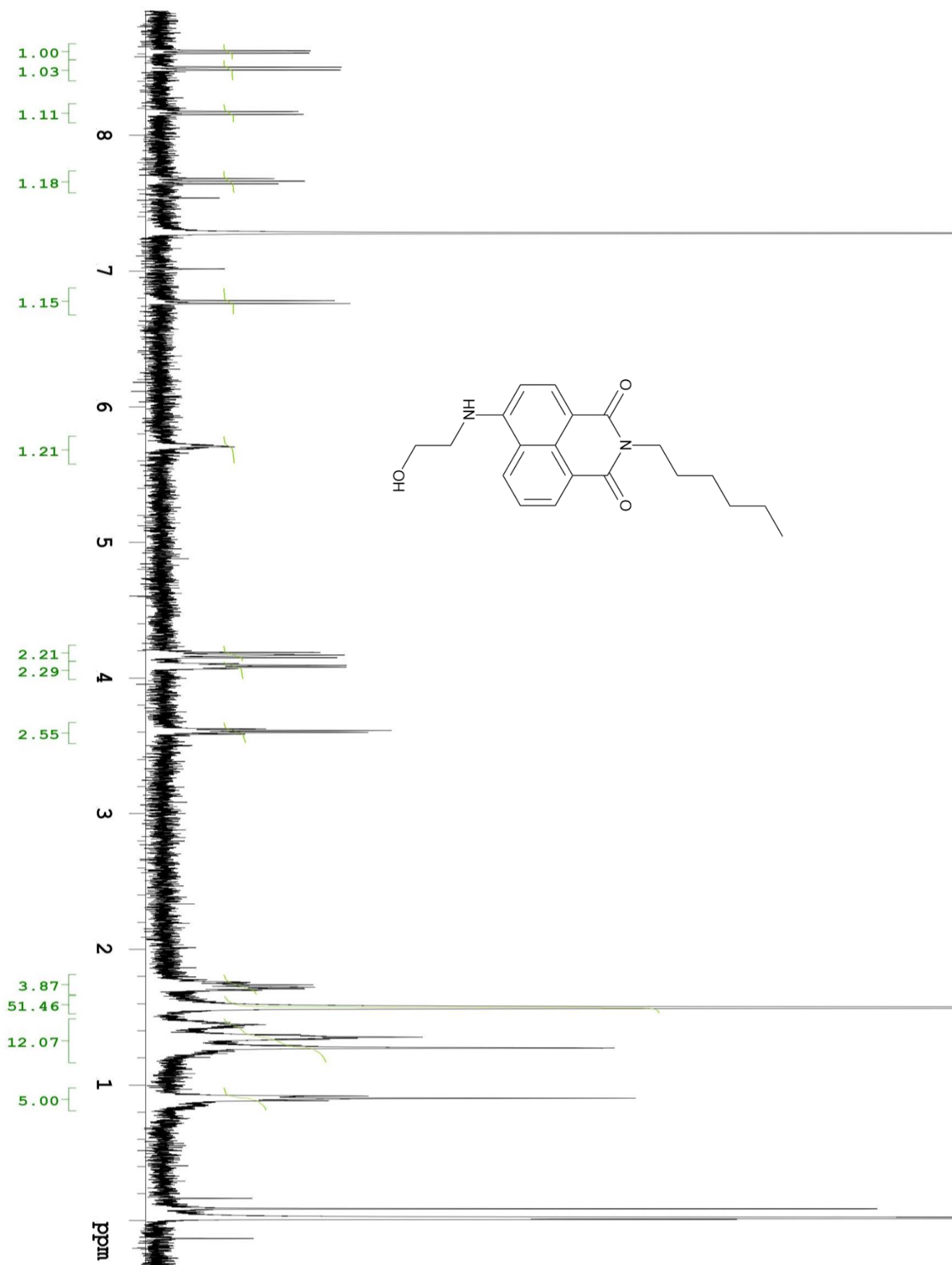
Sample Name
Date collected 2023-08-02

Pulse sequence PROTON
Solvent cdcl3

Temperature 62
Spectrometer Agilent-NMR-vnmrs-400

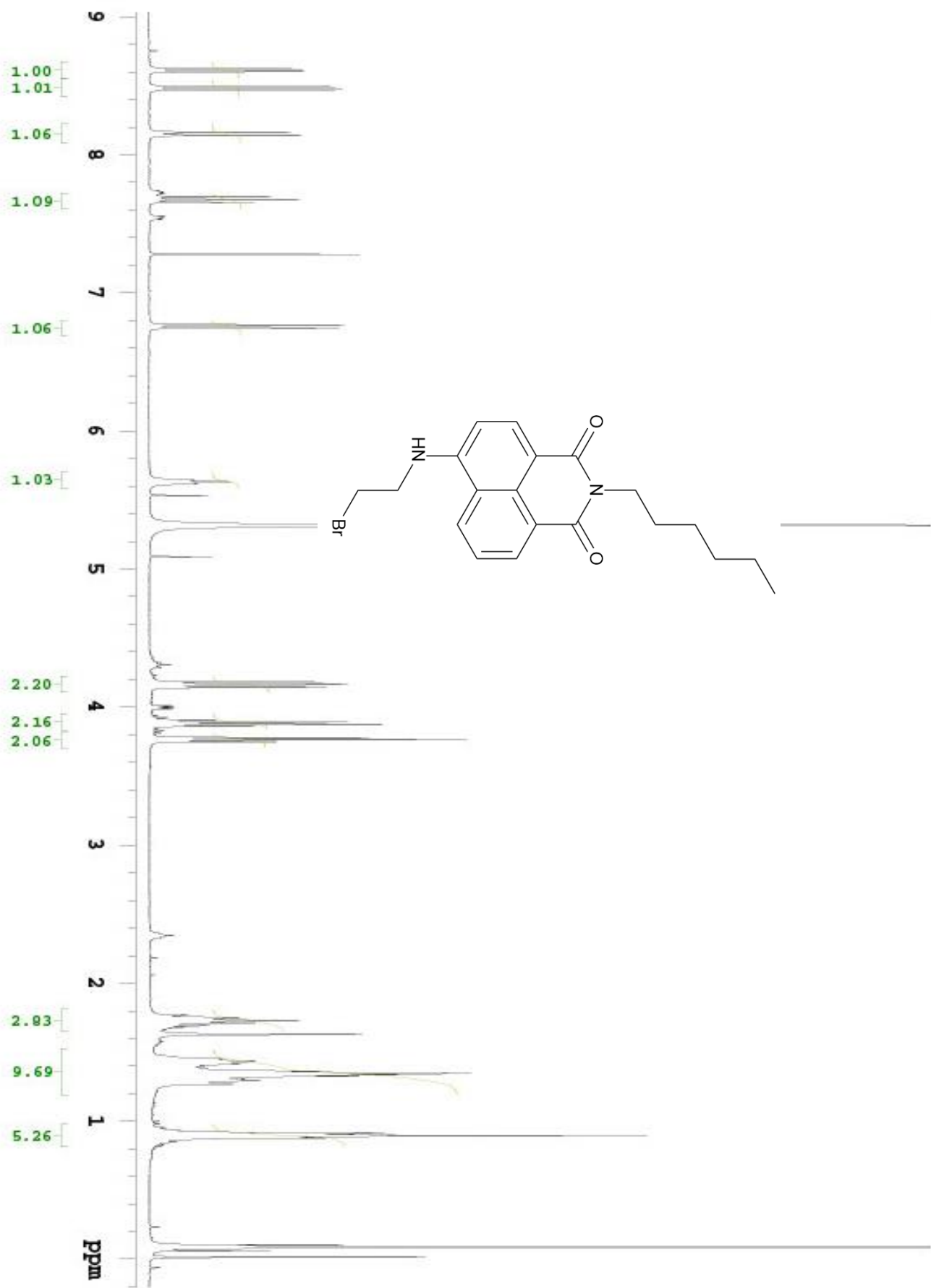
Study owner cjabel
Operator cjabel

5a



Sample Name:
Date collected: **2023-12-21**
Pulse sequence: **PROTON**
Solvent: **cdcl3**
Temperature: **35**
Spectrometer: **Agilent-NMR-vnmr400**
Study owner: **clabel**
Operator: **clabel**

6a



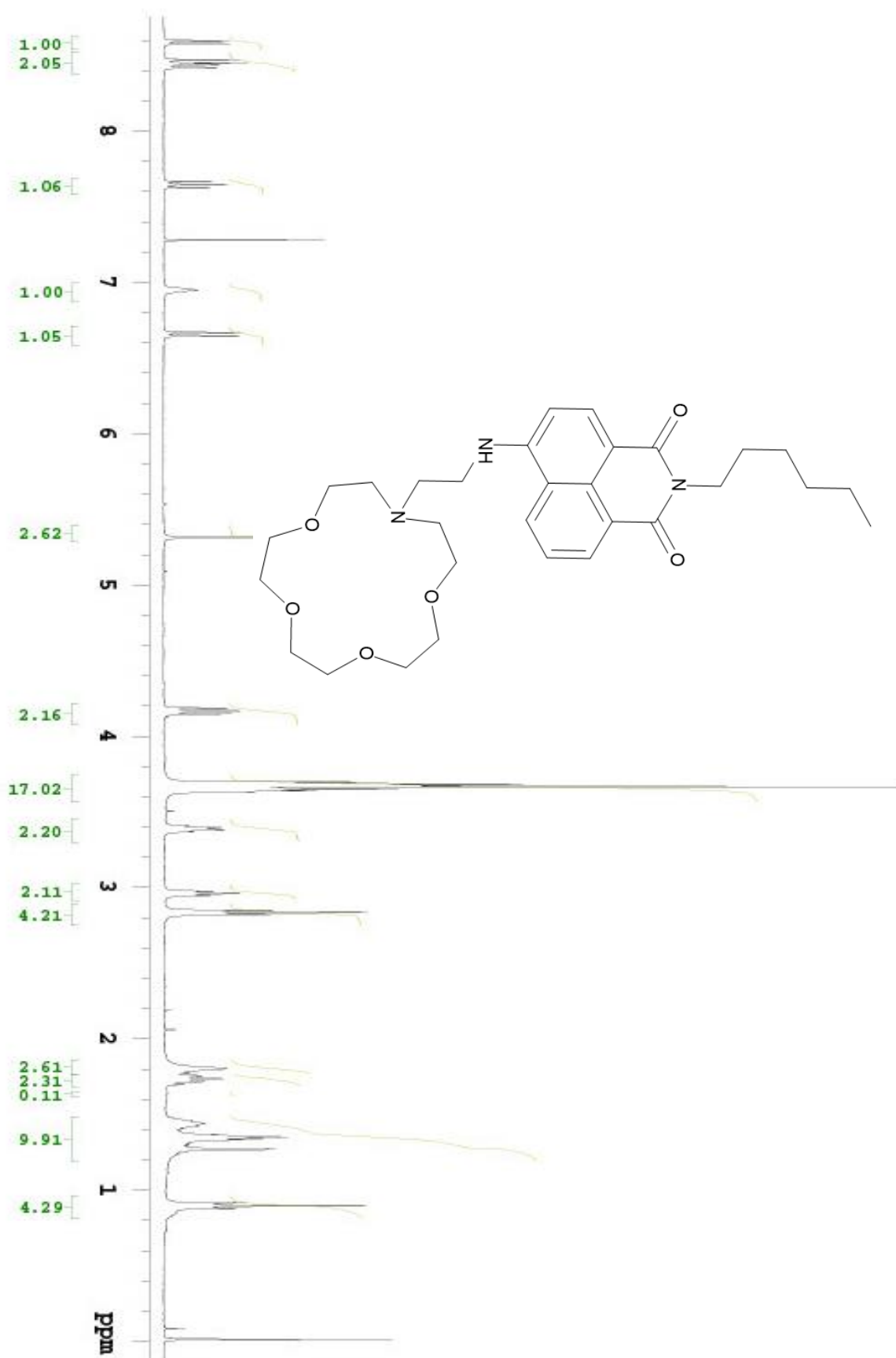
Sample Name:
Date collected: 2023-12-25

Pulse sequence: PROTON
Solvent: cdcl3

Temperature: 35
Spectrometer: Agilent-1HMR-vnmr9400

Study owner: glabei
Operator: glabei

Chemosensor 1



Sample Name
Date collected 2023-12-28

Pulse sequence: PROTON
Solvent: cdcl3

Temperature: 35
Spectrometer: Agilent-NMR-vnmr3400

Study owner: glabei
Operator: glabei

Sample Name
Date collected

2024-01-06

Pulse sequence
Solvent

PROTON
cdd3

Temperature
Spectrometer

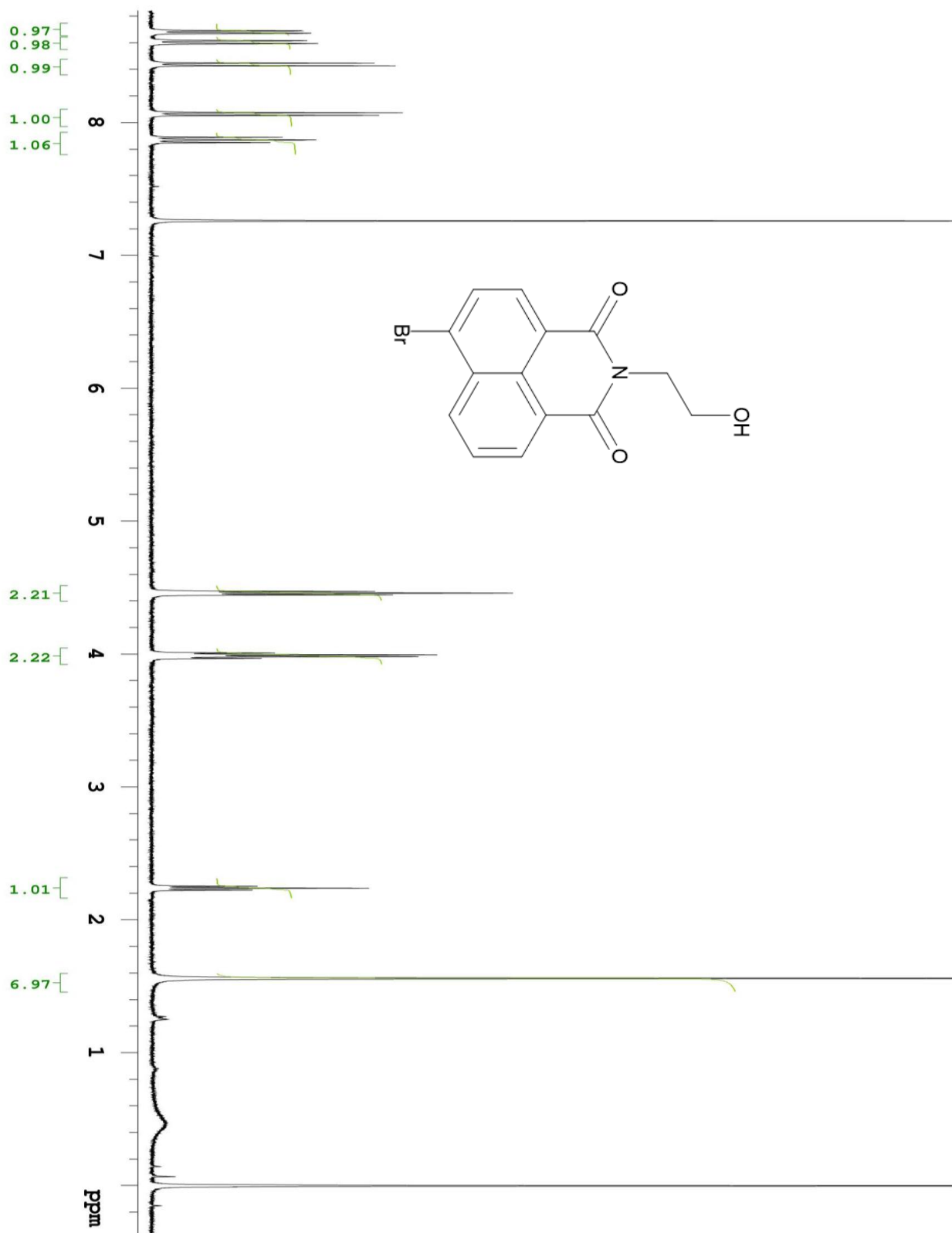
35

Agilent-NMR-rnmrs400

Study owner
Operator

ciabel
ciabel

4b

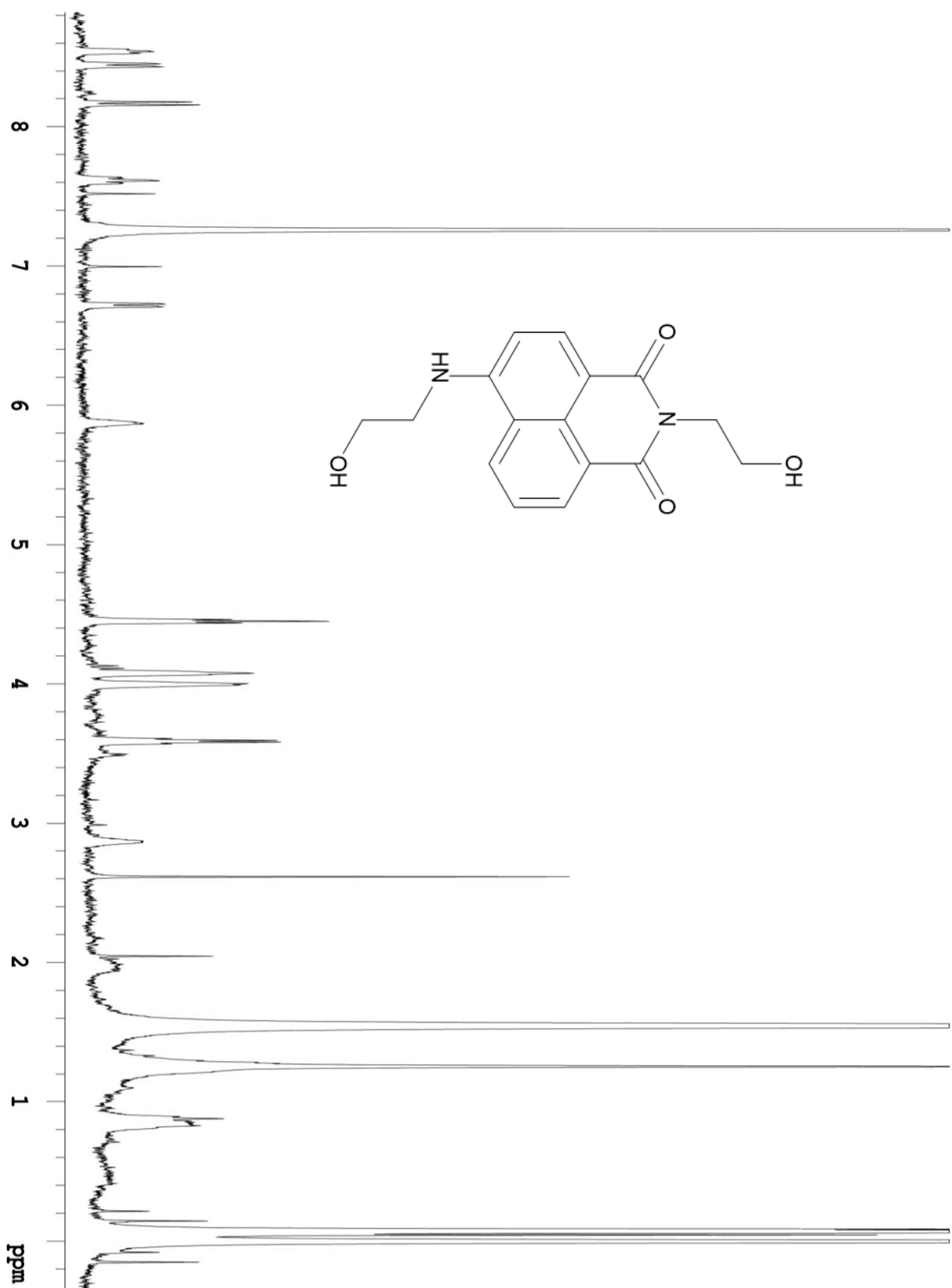
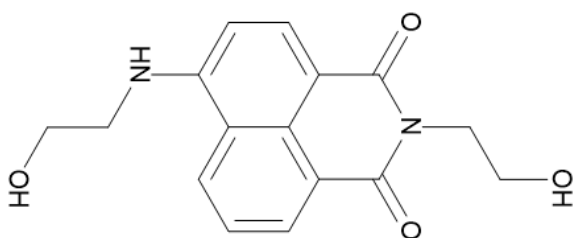


Sample Name
Date collected **2024-01-11**

Pulse sequence **PROTON**
Solvent **cdcl3**

Temperature **35**
Spectrometer **Agilent-NMR-vnmrs400**

Study owner **clabel**
Operator **clabel**



5b

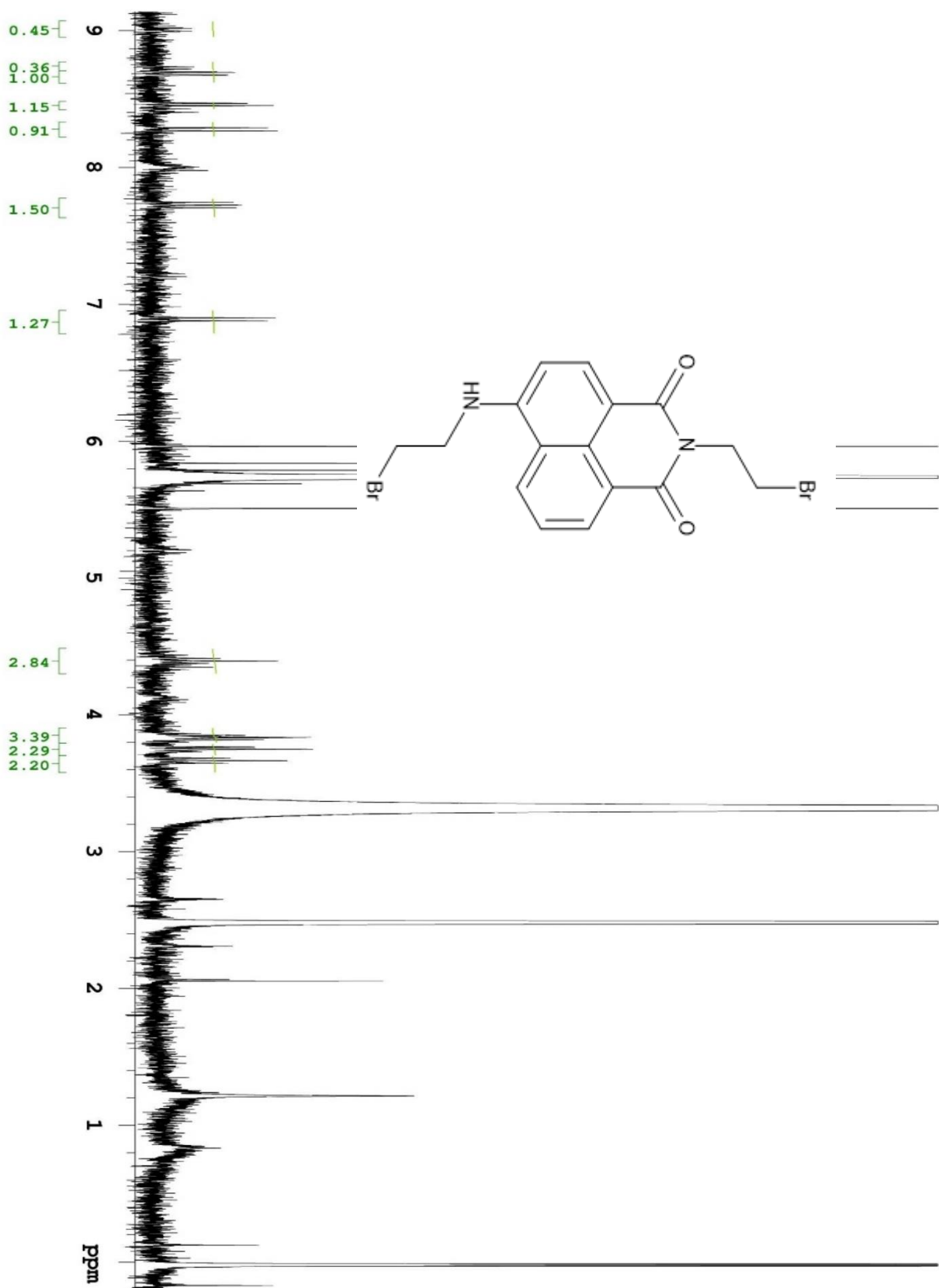
Sample Name
Date collected **2024-01-22**

Pulse sequence **PROTON**
Solvent **dms**

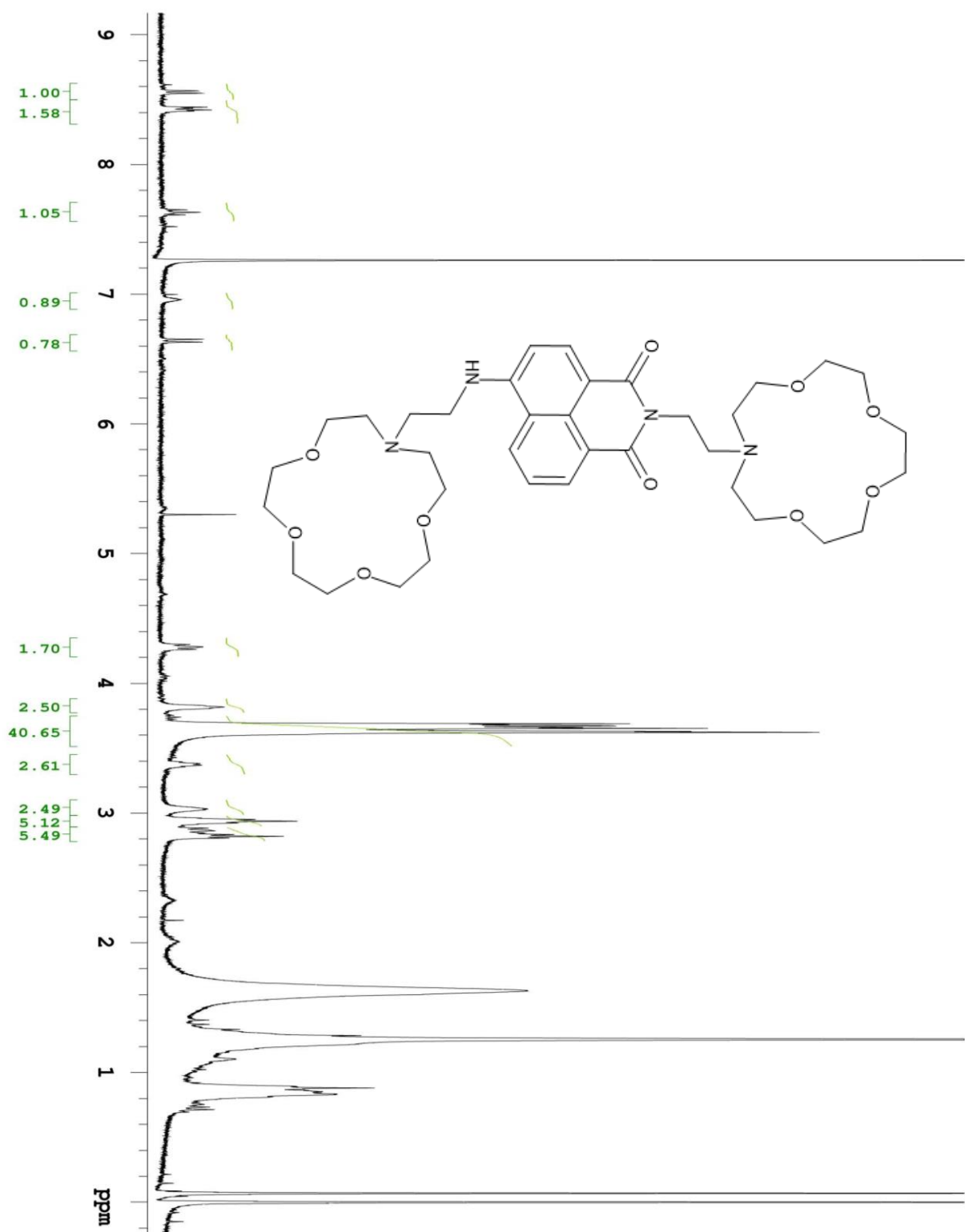
Temperature **22**
Spectrometer **Agilent-NMR-vnmr5400**

Study owner **clabel**
Operator **clabel**

6b



Chemosensor 2



Fractions14-17disub

Sample Name Fractions14-17disub
Date collected 2024-03-05Pulse sequence PROTON
Solvent cdcl3Temperature 25
Spectrometer Agilent-NMR-vnmrs400Study owner clabel
Operator clabel

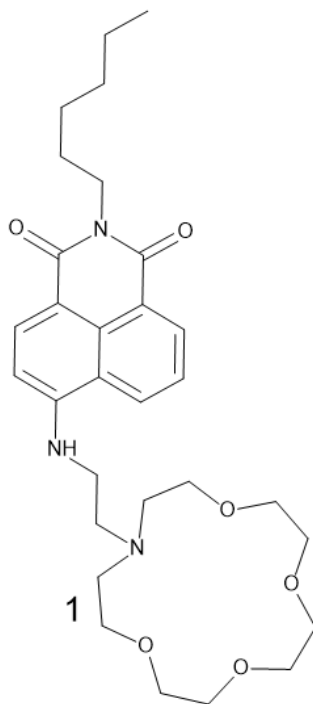
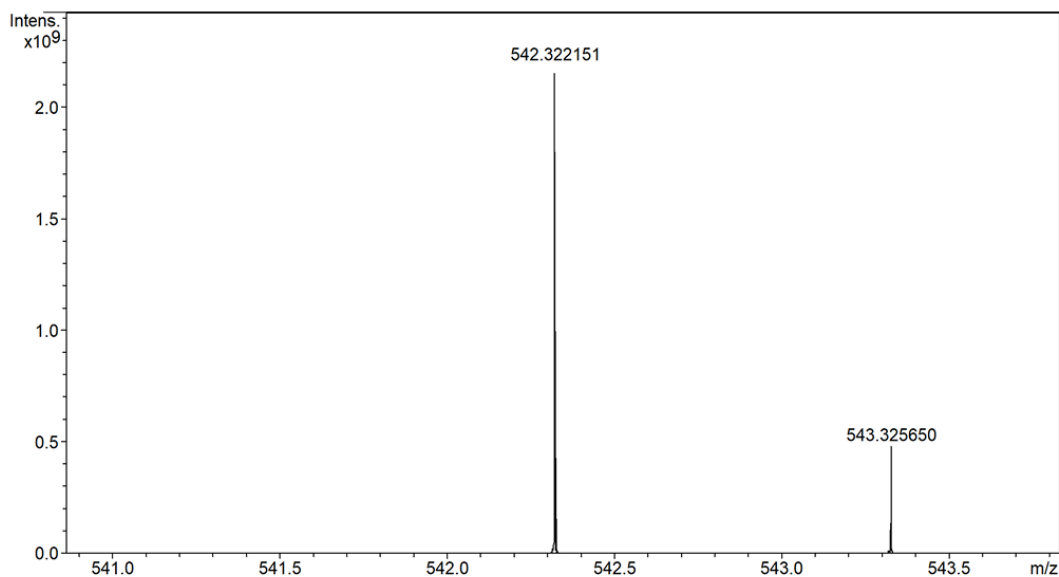
Mass Spectrum List Report

Analysis Info

Analysis Name	D:\MS1 COSMIC\2024\apexdata040424\orhan1_pos_000002.d		Acquisition Date	4/4/2024 9:39:31 AM
Method			Operator	COSMIC
Sample Name	orhan1		Instrument	apex-Qe
Comment	orhan1 in MeOH	C30H43N3O6 H+		

Sample Name	orhan1 in MeOH			
Exact Mass of	C30H43N3O6 H+	=	542.322463	m/z
Mass Observed		=	542.322151	m/z

Difference < 1.0 ppm



Mass Spectrum List Report

Analysis Info					
Analysis Name	D:\MS1 COSMIC\2024\apexdata040424\orhan2_pos_000003.d	Acquisition Date	4/4/2024 10:25:26 AM		
Method		Operator	COSMIC		
Sample Name	orhan2	Instrument	apex-Qe		
Comment	orhan2 in MeOH:THF	C36H54N4O10 H+			

Sample Name	orhan2 in MeOH:THF				
Exact Mass of	C36H54N4O10 H+	=	703.391270	m/z	
Mass Observed		=	703.391244	m/z	

Difference < 1.0 ppm

